
# NAVAL POSTGRADUATE SCHOOL

**MONTEREY, CALIFORNIA**

# THESIS

**CLOCK SYNCHRONIZATION THROUGH TIME-VARIANTUNDERWATER ACOUSTIC CHANNELS**

by

Pascal Gagnon

September 2012

Thesis Co-Advisors: Joseph A. Rice
Grace A. Clark
Roberto Cristi

**Approved for public release; distribution is unlimited**

THIS PAGE INTENTIONALLY LEFT BLANK

| REPORT DOCUMENTATION PAGE | | | Form Approved OMB No. 0704-0188 |
|---|---|---|---|
| Public reporting burden for this collection of information is estimated to average 1 hour per response, including the time for reviewing instruction, searching existing data sources, gathering and maintaining the data needed, and completing and reviewing the collection of information. Send comments regarding this burden estimate or any other aspect of this collection of information, including suggestions for reducing this burden, to Washington headquarters Services, Directorate for Information Operations and Reports, 1215 Jefferson Davis Highway, Suite 1204, Arlington, VA 22202-4302, and to the Office of Management and Budget, Paperwork Reduction Project (0704-0188) Washington DC 20503. | | | |
| **1. AGENCY USE ONLY** *(Leave blank)* | **2. REPORT DATE** September 2012 | **3. REPORT TYPE AND DATES COVERED** Master's Thesis | |
| **4. TITLE AND SUBTITLE** Clock Synchronization Through Time-Variant Underwater Acoustic Channels | | **5. FUNDING NUMBERS** | |
| **6. AUTHOR(S)** Pascal Gagnon, | | | |
| **7. PERFORMING ORGANIZATION NAME(S) AND ADDRESS(ES)** Naval Postgraduate School Monterey, CA 93943-5000 | | **8. PERFORMING ORGANIZATION REPORT NUMBER** | |
| **9. SPONSORING /MONITORING AGENCY NAME(S) AND ADDRESS(ES)** N/A | | **10. SPONSORING/MONITORING AGENCY REPORT NUMBER** | |
| **11. SUPPLEMENTARY NOTES** The views expressed in this thesis are those of the author and do not reflect the official policy or position of the Department of Defense or the U.S. Government. IRB Protocol number ___N/A____. | | | |
| **12a. DISTRIBUTION / AVAILABILITY STATEMENT** Approved for public release; distribution is unlimited | | **12b. DISTRIBUTION CODE** A | |

**13. ABSTRACT (maximum 200words)**

The goal of this work is to develop methodologies for synchronizing the clocks of neighboring nodes of an underwater acoustic network. Clock synchronization requires an estimate of the signaling time delay between the nodes, which is particularly challenging in the presence of multipath propagation through the acoustic communication channel. This thesis focuses on modeling the underwater acoustic communication channel, accounting for the multipath arrivals, and creating a set of signal processing algorithms for estimating the required delay times that enable clock synchronization protocols for the underwater acoustic network. The proposed method involves correlating the responses of the bidirectional channels to exploit the underlying reciprocity. Performed in two stages, a sequence of probe signals is first transmitted to create an ensemble, which contains information about the time-variability of the acoustic communication channel with multipath. From this ensemble, we determine its dominant time-invariant characteristic and use it as a reference datum for the time delay measurements. The second stage consists in performing time-delay estimation of two probe signals exchanged between nodes. The two stages are tested using simulated signal measurements, and actual signal measurements were performed in a fresh-water lake for the first phase only. Both computer simulations and experimental results show the effectiveness of the proposed techniques.

| **14. SUBJECT TERMS** Acoustic communications, Seaweb, Clock synchronization, Impulse response, Underwater communications, Acoustic modem, Ranging | | | **15. NUMBER OF PAGES** 104 |
|---|---|---|---|
| | | | **16. PRICE CODE** |
| **17. SECURITY CLASSIFICATION OF REPORT** Unclassified | **18. SECURITY CLASSIFICATION OF THIS PAGE** Unclassified | **19. SECURITY CLASSIFICATION OF ABSTRACT** Unclassified | **20. LIMITATION OF ABSTRACT** UU |

NSN 7540-01-280-5500

Standard Form 298 (Rev. 8-98)
Prescribed by ANSI Std. Z39.18

THIS PAGE INTENTIONALLY LEFT BLANK

**Approved for public release; distribution is unlimited**

# CLOCK SYNCHRONIZATION THROUGH TIME-VARIANT UNDERWATER ACOUSTIC CHANNELS

Pascal Gagnon
Lieutenant-Commander, Royal Canadian Navy
B.Eng. Royal Military College of Canada, 1999

Submitted in partial fulfillment of the
requirements for the degree of

**MASTER OF SCIENCE IN ENGINEERING ACOUSTICS**
and
**MASTER OF SCIENCE IN ELECTRICAL ENGINEERING**

from the

**NAVAL POSTGRADUATE SCHOOL**
**September 2012**

Author: Pascal Gagnon

Approved by:

Joseph A. Rice
Thesis Co-Advisor

Grace A. Clark
Thesis Co-Advisor

Roberto Cristi
Thesis Co-Advisor

Daphne Kapolka
Chair, Engineering Acoustics
Academic Committee

R. Clark Robertson
Chair, Department of Electrical
and Computer Engineering

THIS PAGE INTENTIONALLY LEFT BLANK

# ABSTRACT

The goal of this work is to develop methodologies for synchronizing the clocks of neighboring nodes of an underwater acoustic network. Clock synchronization requires an estimate of the signaling time delay between the nodes, which is particularly challenging in the presence of multipath propagation through the acoustic communication channel. This thesis focuses on modeling the underwater acoustic communication channel, accounting for the multipath arrivals, and creating a set of signal processing algorithms for estimating the required delay times that enable clock synchronization protocols for the underwater acoustic network. The proposed method involves correlating the responses of the bidirectional channels to exploit the underlying reciprocity. Performed in two stages, a sequence of probe signals is first transmitted to create an ensemble, which contains information about the time-variability of the acoustic communication channel with multipath. From this ensemble, we determine its dominant time-invariant characteristic and use it as a reference datum for the time delay measurements. The second stage consists in performing time-delay estimation of two probe signals exchanged between nodes. The two stages are tested using simulated signal measurements, and actual signal measurements were performed in a fresh-water lake for the first phase only. Both computer simulations and experimental results show the effectiveness of the proposed techniques.

THIS PAGE INTENTIONALLY LEFT BLANK

# TABLE OF CONTENTS

# LIST OF FIGURES

THIS PAGE INTENTIONALLY LEFT BLANK

# LIST OF TABLES

THIS PAGE INTENTIONALLY LEFT BLANK

# LIST OF ACRONYMS AND ABBREVIATIONS

| | |
|---|---|
| OSI | Open Systems Interconnection |
| DSP | Digital Signal Processor |
| TSVP | Time Synchronization for time-Varying Propagation underwater network Protocol |
| AUV | Autonomous Underwater Vehicle |
| WSSUS | Wide-Sense Stationary Uncorrelated Scattering |
| RPI | Reference Pulse Interval |
| SPI | Synchronizing Pulse Interval |
| LFM | Linear Frequency-Modulated |
| PDF | Probability Density Function |
| SMART | Smart Modem Acoustic Release Technology |
| SDHC | Secure Digital High Capacity |
| AGC | Automatic Gain Control |

THIS PAGE INTENTIONALLY LEFT BLANK

# EXECUTIVE SUMMARY

Clock synchronization among network nodes becomes necessary when data from multiple nodes are to be co-processed. In the context of surveillance networks, synchronization of the nodes' clocks is directly related to the accuracy of the localization of a potential target. Clock synchronization is achieved by evaluating and then correcting the skew and offset of the internal clock of a single node. The skew of a clock is the oscillator frequency difference between two synchronizing clocks, whereas the offset is the time difference at a specific point in time between two clocks.

Clock synchronization is especially important for high-latency communications such as those in underwater acoustic networks in which data from separate nodes take variable amounts of time to reach the main processing node. The challenge in underwater acoustic clock synchronization lies in correctly estimating the time delay between the transmission of a signal from a node and the reception of that signal by another node. For the acoustic communications problem, the propagation medium introduces environmental factors such as high latency, multipath, scattering, refraction, transmission loss, noise and non-reciprocity. These factors have significant effects on the channel impulse response. The individual multipath arrival amplitudes and the arrival times can also vary greatly depending on the surface conditions and the directivity of the transducers. For some environmental conditions, the first or other multipath arrivals may be greatly attenuated or absent altogether.

The aim of this thesis is to examine how time-variability of the impulse response impacts clock-synchronization and how it can be avoided or mitigated in a spatially static underwater network. The Time Synchronization for High Latency (TSHL) protocol developed by Syed and Heidemann in [1] is used as the basis for this research. The protocol is adapted to account for time-variability of the channel impulse response.

In the absence of a fit-for-all underwater statistical model, channel soundings are a good alternative to the lack of prediction capability. They are direct measurements of the time-varying impulse response of a propagation medium and replace general

assumptions about the prevailing channel between two nodes. A series of pulses is sent through the channel at a set interval. The receiver analyzes the received series and compiles its own local channel characteristics from it.

Our approach relaxes the assumption in TSHL of a stable propagation delay between the synchronizing nodes. It also relaxes the reciprocity assumption for the channel. Instead, we repeatedly measure the response of the channel over a period of time to statistically define the communication channel to better estimate the propagation delay and its skew. This approach could also be defined as adding channel sounding to the TSHL protocol. Our model keeps the two-stage approach developed by TSHL, correcting for the skew first followed by the offset.

In the skew-correction stage, we analyze a series of chirp responses to identify the least time-varying multipath present in the channel between the two nodes. Based on the known chirp transmission interval, linear regression is performed on the measured interval of arrivals of that identified multipath detected within each chirp response. The slope of the resulting best-of-fit straight line represents the skew of the clock's receiver node compared to the originating or reference node.

The second stage consists of an exchange of time-stamp messages between the two nodes, where we assume a time-varying, one-way propagation delay between the two nodes. The challenge in this stage consists in determining the difference in propagation delays. This is accomplished by performing, at one of the nodes, a time-delay estimate using the chirp responses of the channel sounding of both one-way propagation paths.

The Bellhop and VirTEX underwater environment models are used to simulate a simple communication channel in Matlab. Variability is introduced in the model by modifying the state of the surface and rotating one of the nodes between the transmissions of the chirps. The aim of the simulations was to prove our conceptual approach prior to conducting an in-water experiment and to demonstrate the effect of time-variability on our clock-synchronization process. The simulation verified the theory of our approach as it precisely determined the difference in propagation delays and clock offset.

The first stage of the algorithm was then tested in the Del Monte Lake situated on the NPS campus. The general concept of the experiment consisted of transmitting and recording a series of chirps between two acoustic modems. The characteristics (duration and modulation) of the chirp were modified between the transmissions of the transmitted chirp series to analyze the impact of the chirp selection on the protocol. The digital recordings were recovered and analyzed using the same algorithms exercised in the simulation. The second stage of the algorithm was not tested since it would require modifying the firmware of the acoustic modems to program the message exchange protocol.

Overall, the results from the experiment demonstrate some time variability in the tested channel. The first arrival is always present and strong. However, the following arrivals are observed to be gradually less stable as they increasingly interact with the channel boundaries. The algorithm is able to identify various multipaths based on the detected arrivals and determines the most stable one based on the correlation coefficient of a model fit to the time-of-arrival estimates.

Additional experiments are required to fully prove the developed algorithms and select the optimal parameters, such as the probe signal characteristics. Once completely tested, the addition of this capability to an underwater acoustic network should allow it to keep the clocks of the nodes synchronized. This synchronization should improve the reliability of the network when deployed or used for long periods of time.

[1] A.A Syed and J. Heidemann, “Time Synchronization for High Latency Acoustic Networks,” in *Proc. Of IEEE Conference on Computer Communications (Infocom)*, Barcelona, Spain, Apr. 2006.

THIS PAGE INTENTIONALLY LEFT BLANK

# ACKNOWLEDGMENTS

The completion of this thesis not only means the conclusion of my postgraduate studies but also the end of an amazing opportunity and experience at the Naval Postgraduate School. I wouldn't have been able to make it this far without the help and support from so many colleagues, friends and family. I would especially like to thank:

To my initial theses advisor, Joe Rice who helped me to determine my thesis topic and patiently guided me to its conclusion.

To Dr. Grace Clark who really got this thesis going. Your guidance, enthusiasm and support made even the hardest part of this thesis fun to work on.

To Roberto Cristi, my "go-to" professor for quick answers and for stepping in as a last-minute co-advisor.

To Chris Fletcher and Bob Creber from SPAWAR, San Diego for helping me to understand how an acoustic underwater network is deployed and actually works.

To Ken Scussel and Mike Coryer from Teledyne Benthos for explaining some of the technical features of the modems and for providing advice when conducting the experiment in Del Monte Lake.

To Sam Barone for moral support and coffee, lots of coffee.

To Marnix and Tim, the other two members of the Canadian, Netherland and American mutual support coalition in SP-008.

To my parents who have always encouraged and supported me through all of my adventures.

To the most important people in my life, my wife Kylie and my children, Naomi and Jeremy. Your incredible and ever-lasting support is the main reason why I have made it this far.

THIS PAGE INTENTIONALLY LEFT BLANK

# I. INTRODUCTION

## A. REQUIREMENT FOR CLOCK SYNCHRONIZATION

Clock synchronization in distributed sensor networks has been a research topic for many years. Synchronization among network nodes becomes necessary when data from multiple nodes are to be co-processed. In the context of target detection and triangulation, the synchronization of the nodes' clocks is directly related to the accuracy of the localization of a potential target.

The majority of recent developments in the literature involve wireless radio networks where signal propagation is almost instantaneous (speed of light). In most of the literature, clock synchronization is accomplished via the exchange of time-stamped messages between two nodes. This is achieved by evaluating and then correcting the skew and offset of the internal clock of a single node. The accuracy of clock synchronization is directly related to the accuracy of the measured propagation time delays among the nodes.

## B. CLOCK SYNCHRONIZATION IN THE UNDERWATER ACOUSTIC CHANNEL

Clock synchronization is especially important for high-latency communications such as those in underwater acoustic networks where data from separate nodes take variable amounts of time to reach the main processing node. The challenge in underwater acoustic clock synchronization lies in correctly estimating the time delay between the transmission of a signal from a node and the reception of that signal by another node. For the acoustic communications problem, the propagation medium introduces environmental factors such as high latency, multipath, scattering, refraction, transmission loss, noise, and non-reciprocity. These factors have significant effects on the channel response. Prior to performing clock synchronization, we must address the complex time delay estimation issues associated with the response of the channel. The idealized model for the channel impulse response is a sequence of impulses representing the multipath arrivals caused by the channel. In theory, we can estimate the time delay

between transmission and reception by identifying a reference arrival (e.g. the first arrival or another reliable arrival). However, the individual multipath arrival amplitudes and the arrival times can vary greatly depending on the surface conditions and the directivity of the transducers. For some environmental conditions, the first or other multipath arrivals may be greatly attenuated or absent altogether. This makes the identification of a reference arrival very difficult.

While the previously stated difficulties associated with clock-synchronization protocols in an underwater network are important, the extreme bandwidth and latency limitations of underwater communications constrain the implementation of synchronization protocols that involve negotiation or arbitration. Most underwater acoustic networks can only achieve very low data communication rates and care must be taken to limit the amount of information exchanged between the nodes of the network. Associated with this limitation is the finite power supply at each node. To maximize the operational utilization of a node, the number of transmissions and their associated message length must be limited. In the context of clock synchronization, the communications exchanged between the synchronizing nodes must be minimized, while the length of time between the need to repeat the clock synchronization algorithm should be maximized.

The aim of this thesis is to examine how time variability of the impulse response impacts clock-synchronization and how it can be mitigated in a spatially static underwater network. The Time Synchronization for High Latency (TSHL) protocol developed by Syed and Heidemann in [1] is used as the basis for this research. It is often referred to as the source of other work in the literature, like this research.

Originally, TSHL is designated for spatially fixed underwater networks. In this research it is adapted to account for time variability of the channel impulse response and tested using computer simulations. Actual acoustic signal measurements acquired under controlled conditions in a fresh-water lake serve to verify the physical assumptions that are the basis of the protocol.

This thesis is organized as follows. The general concepts associated with clock-synchronization and the variability of the underwater communication channel are introduced in Chapter II and III. Our proposed clock-synchronization algorithms accounting for time-variability in the channel are presented in Chapter IV. These algorithms are then simulated in Chapter V and some of them tested in an actual underwater environment in Chapter VI. Finally, the recommendation and conclusions are given in Chapter VII and VIII.

THIS PAGE INTENTIONALLY LEFT BLANK

# II. CLOCK SYNCHRONIZATION

## A. THE COMPUTER CLOCK

A computer clock is an ensemble of hardware and software components used to provide an accurate, stable and reliable time-of-day function to the operating system and its clients [2]. From a hardware point of view, most clocks are based on a mechanism that oscillates at a precise constant frequency. The precision of the oscillator to generate this frequency is defined as its tolerance, and since it is usually very low, it is expressed in terms of parts-per-million (ppm). How well it can maintain this set frequency is defined as the stability of the clock. The oscillating mechanism can take the form of a simple mechanical pendulum, or the vibrations of electrons in an atom. These two technologies are situated at opposite ends of the spectrum in terms of precision, stability, complexity and cost. In the vast majority of cases, the middle-of-the-road solution is to use a man-made quartz crystal as the oscillating mechanism.

By knowing the oscillating frequency of the mechanism, a unit of time can be linked to a set number of oscillation periods. In the case of a computer clock, a simple counter will send an interrupt message incrementing the clock by one time unit following a pre-determined number of oscillations. Sending this interrupt resets the counter to 0 and reinitiates the process.

## B. THE QUARTZ CRYSTAL OSCILLATOR

### 1. General Description

More than 2 billion quartz crystal oscillators are manufactured annually [2]. They are used in consumer electronics such as wristwatches, mobile phones and computers, and in equipment requiring greater precision such as test and measurement instruments. Quartz crystal is abundant in nature and is easy to grow in large quantities, at low cost, and with relatively high purity. It is the piezoelectric property of the quartz crystal which makes it a material of choice for use as a stable resonator in oscillators. Its high Q value makes it an excellent material for use as an oscillator [2]. A quartz crystal can be manufactured in various structures and cuts, which define its own operational

characteristics. One such characteristic is the resonant frequency which can be from a few tens of kilohertz to tens of megahertz.

### 2. Quartz Crystal Instabilities

A quartz crystal often includes impurities which lead to variations in the resonance frequencies. This is especially true for less expensive oscillators found in most electronic devices, where the frequency can vary up to 40 ppm between two clocks [3]. The resonating frequency of a quartz crystal is subject to many types of instabilities which can affect its precision and accuracy [4]. These include aging, noise, and frequency changes depending on temperature, acceleration, ionizing radiation, power supply voltage, etc. By knowing how these instabilities affect a clock, it is possible to correct for them using hardware or software solution. As an example, the real-time clock used on Benthos Teledyne acoustic modems is temperature compensated [5].

## C. THE NEED FOR A REFERENCE TIME

Every single device in a network will have at least one local clock, the time of which will be different from another unless we provide proper synchronization. Depending on how much the times differ, the following fundamental operations performed by a node in a wireless sensor network may or may not be possible [3].

There are a number of issues strictly related to clock management, and they are listed next.

### 1. Data Fusion

This is one of the principal benefits to be derived from a sensor network, where the goal is to observe and report on events. To coherently integrate and process event information from multiple sensors in a meaningful way, all data must be referenced to a standard time.

### 2. Power Management

One way to manage and save energy in a network is by the implementation of a duty cycling protocol. Instead of leaving a node operational for a continuous period of

time, it can be programmed to sleep and wake-up at a set time interval. While in sleep mode, the node saves energy by keeping only essential systems operating and expending minimum power. To permit communication between two nodes, both of them need to be awake at the same time. Here lies the importance that both nodes operate on a synchronized clock, such that they can simultaneously switch between operating modes.

### 3. Transmission Scheduling

Some network protocols allow a node access to a network by implementing a set schedule for when a specific node can transmit (i.e., the time-division multiple access protocol ) [3]. From this schedule, only one node can transmit at a time, reducing the risk of collisions within the network. Another advantage of such a protocol is the reduction of the message overhead that is usually required to control the communication flow within the channel, therefore increasing the available bandwidth. The main requirement for this kind of protocol is that every node in the network must use synchronized clocks to start and stop their transmissions on a common distributed schedule.

### 4. Master-slave Relationship

The above operations have a mutual requirement: the internal reference clock of every node in the network must be synchronized. For synchronization to exist, the concept of a master-slave relationship must be introduced in the network. In the case of a sensor network, a node is designated as master and its internal clock is used as a reference by all the other nodes, designated as slaves. To avoid having to repeatedly re-synchronize the clocks of the network, the master node is often equipped with a more stable and precise clock than the other nodes or will have the capability to synchronize with an external reference time such as the one provided by the GPS. Having an accurate master clock is desirable in a sensor network but is not as critical as having all the clocks of the network synchronized with the master.

## D. CLOCK MODEL

Each device or node in a sensor network has its own clock. The time measured by clock A usually presents random errors, but on average it can be represented by a linear function of the form

$$C_A(t) = f_A t + b_A \tag{1}$$

where the term $f_A$ represents the skew and $b_A$ the offset of clock $C_A$ compared to its reference or master clock $C_B$. Throughout this paper B denotes the reference node and A the synchronizing node. In an ideal situation with no errors or drifts, we have $C(t) = t$. The skew of a clock $f_A$ is the oscillator frequency difference between $C_A$ and $C_B$. The offset $b_A$ is the time difference at a specific point in time between the two clocks. Figure 1 is a graphical representation of a perfect reference clock combined with both a slower and faster slave with respective offset clocks.

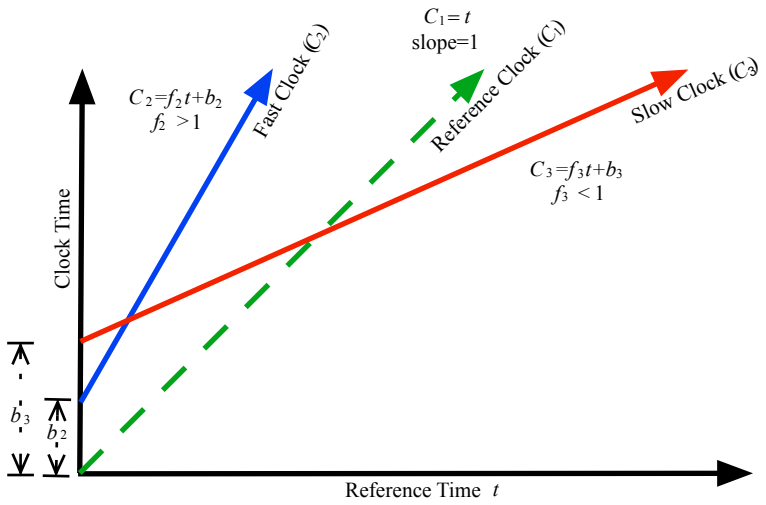


Figure 1. Clock model of a fast ($C_2$), reference ($C_1$), slow clock ($C_3$) and their associated equations.

## E. SOURCES OF ERROR IN CLOCK SYNCHRONIZATION

In a perfect, ideal environment with no delayed responses, clock synchronization is simple. Node B sends its current time to node A, which adjusts its own clock

accordingly. In an actual network, many steps are required to accomplish this exchange of information. Associated with each of these steps is a systemic time delay which can be either deterministic or stochastic.

The following is a list of the various delays generated by the transmission of a timing message between two nodes [1] and illustrated using the open systems interconnection (OSI) model in Figure 2. The OSI model structures a communication system in terms of functional layers. Each layer can only communicate with the layer above or under it within a communication device. In order for a communication system to exist, two devices or nodes must share the same layered structure.

### 1. Send Time

Send time is the time delay from generating the timing message at the synchronizing node by its software as transfers through the application, transport and network layers on the sender side illustrated in Figure 2. This delay results from the execution of software operations and is a fixed time in most devices.

### 2. Access Time

This is the contention time to access the channel. It is highly variable and depends on the MAC protocol used and how busy the channel is when the node is attempting to access it.

### 3. Transmission and Reception Time

This is the time to send and receive the entire message by the transducer. This is a deterministic delay, which depends on the size of the message sent and the bandwidth of the link. This is illustrated by the four green squares in Figure 2, each representing a packet.

### 4. Propagation Time

The propagation is the time required for the timing message to travel between the two nodes. The high-latency nature of water as a communication medium makes determining this delay very difficult. This problem is further explained in Chapter III.

### 5. Encoding and Decoding Time

This is the time required for the digital signal processor (DSP) in the acoustic modem to encode/decode the message to/from the received acoustic signal. This is a short and deterministic delay.

### 6. Receive Time

Similar to the send time, this is the delay for the software to process the received timing message through the upper layers of the OSI model as illustrated in Figure 2.

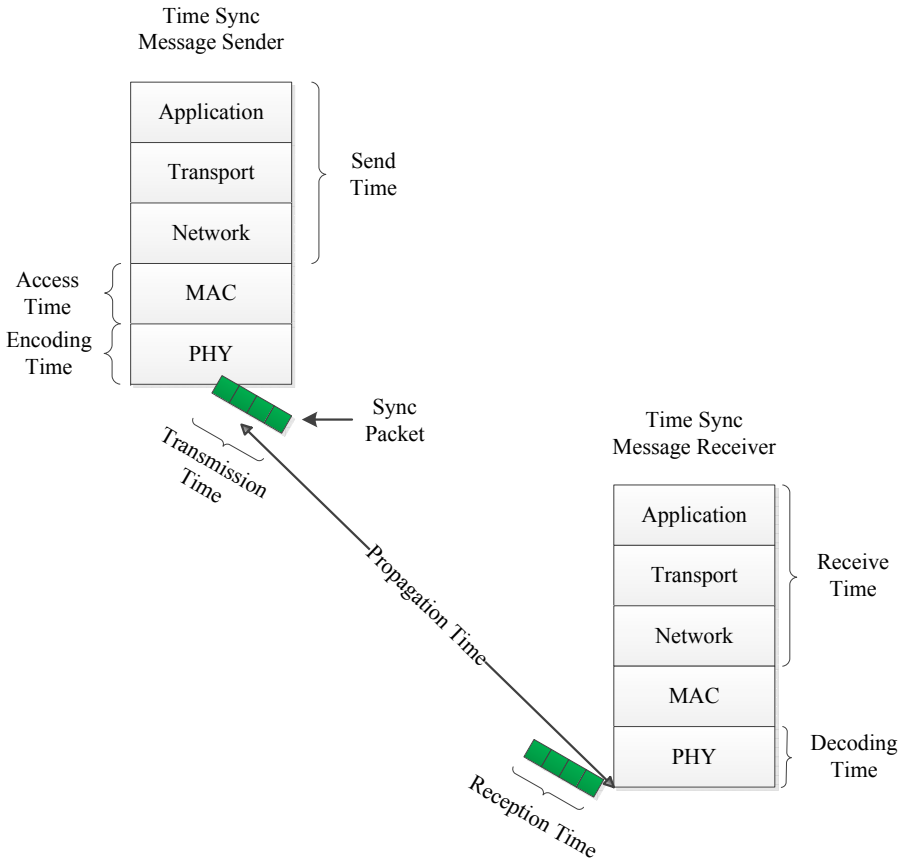


Figure 2. Sources of error in estimating message latency explained using the OSI model. After [1].

To measure and eliminate some of the uncertainties associated with these delays, multiple messages need to be exchanged between the two nodes, adding yet more delays and complexity to the overall process. In some sense, clock synchronization in a sensor network can be regarded as the process of accounting for the effects of unknown delays in the overall communication process [3].

## F. CLOCK SYNCHRONIZATION BASICS

From Equation 1, we see that two parameters (skew and offset) need to be corrected to synchronize a local clock to a reference. In general, the process to execute this correction is achieved by transferring a set of timing messages between the two nodes as shown in Figure 3 and referred to as the two-way message exchange (or sender-receiver synchronization) [6].

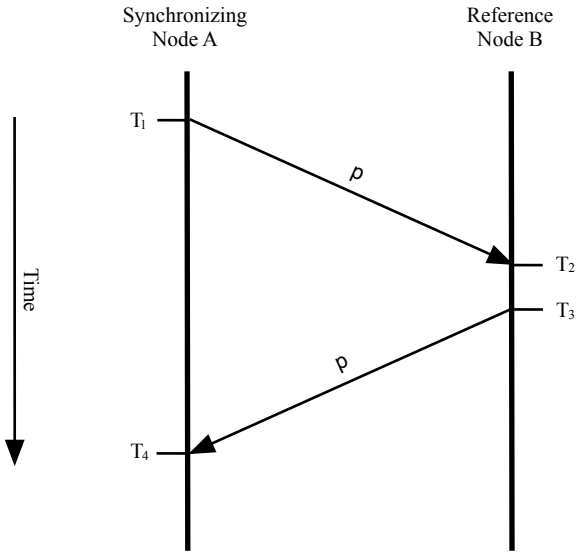


Figure 3. Two-way message exchange of timing messages between the synchronizing (A) and reference (B) nodes. After [1].

Most authors use Figure 3 to describe the basics of clock synchronization protocols. The literature usually assumes a reciprocal and symmetric communication channel where the one-way propagation delay can be determined by averaging the total propagation time of the two message exchanges. Why Figure 3 can be amended to illustrate a time-varying propagation delay, such that the signal propagation delay between node A and B can be different from the one from B to A, is discussed in the next chapter. A solution to address this non-reciprocity is proposed in Chapter IV.

From Figure 3, the total propagation time can be mathematically modeled as

$$(T_4 - T_1) - (T_3 - T_2) = 2p = P. \tag{2}$$

Assuming a constant propagation delay and zero or negligible skew, we can determine the offset of $C_A$ from a single exchange of time-stamped messages such as illustrated in Figure 3. Once the propagation delays have been determined, the offset $b_A$ can be calculated from one of the following:

$$T_2 - T_1 - p = b_A \tag{3}$$

$$T_4 - T_3 - p = -b_A. \tag{4}$$

The offset $b_A$ from Equation 3 changes sign in Equation 4 since the offset sign is relative to which node it is compared with.

By repeating the exchange of time-stamped messages, the clock synchronization protocol can also determine the clock skew using this formulation. The Time Synchronization for Time-Varying Propagation Underwater Network (TSVP) [7] keeps track of the time-stamps and calculates the clock skew using linear regression.

Another well-known timing signaling approach is the one-way message dissemination method [6]. The master node broadcasts its timing information to all the nodes in its vicinity at a set time interval. A slave node collects and saves all the timing information in a matrix to calculate, using a least-squares estimator, the skew and offset of the local clock compared to the reference clock. This method assumes a fixed propagation delay, but the effect of this assumption is mitigated by the fact that the least-squares estimator in fact averages these delays. This methodology is used by the flooding time synchronization protocol (FTSP) [8]. Although this approach requires multiple broadcast messages from the master node, it can synchronize a multitude of slave nodes simultaneously and requires minimal channel access negotiation between the nodes.

How these two signaling approaches are combined and used in two different stages to produce a clock synchronization protocol is described in Chapter IV.

## G. LIMITATION TO CLOCK SYNCHRONIZATION

It is possible to keep all local clocks of a network very precisely synchronized by simply updating them on a periodic basis. However, this scenario is unrealistic and would compromise the efficient use of the node's two limited resources [6], energy and bandwidth, as explained in the following.

### 1. Energy

In general, devices found in sensor networks, even underwater ones, are limited in size and, therefore, restricted in the amount of energy they can hold. In order to maximize its battery and operational life, clock synchronization must be achieved while

preserving energy for normal operations. Since transmitting is an energy-consuming operation, a clock-synchronization protocol must limit the number and the length of the messages exchanged within the network.

### 2. Bandwidth

Underwater networks have limited bandwidth and are restricted to a relatively slow transmission data rate. Clock synchronization is a network support feature and not the main role of a network node. Limiting the bandwidth used for clock synchronization helps to maximize the utilization of the node for its intended main purpose.

A balance based on the trade-offs between the desired clock synchronization precision and the limited network resources must ultimately be achieved to maximize the efficiency of the network.

THIS PAGE INTENTIONALLY LEFT BLANK

# III. VARIABILITY OF THE UNDERWATER COMMUNICATION CHANNEL

The underwater acoustic channel is a challenging communication medium. It can be thought of as a long slim pipe, with the poor physical link quality of a mobile terrestrial radio channel, and the high latency of a satellite channel [9]. Technologies developed for wireless radio communications are often used as the basis for underwater acoustic communications. The ocean shares with the over-the-air medium many of the same impairments that make wireless communications difficult such as multipath, scattering, noise, attenuation, and fading. The difficulties introduced by these characteristics are magnified in the ocean due to the high latency of the medium. Acoustic signals propagate five-orders-of-magnitude slower in water compared to over-the-air RF signals, with speeds of $1.5 \times 10^3$ m/s and $3 \times 10^8$ m/s, respectively. In addition, greater absorption at higher acoustic frequencies limits the available bandwidth, leaving only lower frequencies, which are susceptible to channel fading due to multipath.

Underwater acoustic research usually takes into account the above-mentioned intricacies of the medium. However, most practical solutions make the assumption that the environment is stable over relatively short periods of time. Nevertheless, signal fluctuations can occur due to transceiver motion or inherent changes within the propagation medium. These changes are due to numerous phenomena which, depending on their time scale, might or might not affect the instantaneous quality of the communication channel. They will also have a different impact depending on whether the channel is in deep or shallow water. The shallow-water channel is recognized as being the most difficult due to its time-varying impulse response. This greatly affects the signal propagation delay and impacts the clock synchronization effort.

## A. TRANSDUCER MOTION

In the underwater environment there is always some motion present in the system [9]. Motion can affect the impulse response's frequency spectrum (via the Doppler

effect), strength of the arrival paths, or in the worst case, the complete disappearance of it due to one of the transceivers entering a shadow zone where no communication path exists between two communicating nodes.

The Doppler effect will cause frequency shifting as well as additional frequency spreading. The amount of spectral shift is proportional to the ratio of the relative transmitter-receiver velocity to the speed of sound [9]. Since the speed of sound in the water is relatively slow (1500 m/s), a transducer's motion from waves, currents, tides, and platform motion will be enough to impair the communication channel. Furthermore, unlike wireless communications systems in the air, it has been shown that assumption that the underwater acoustic channels are subject to wide-sense stationary uncorrelated scattering (WSSUS) does not always apply [10].

The rotation of a transducer is another dimension of motion that can affect the impulse response of the channel. As shown in Figure 4, in a multipath environment, the beam pattern of a transducer influences the directivity index for both launch angle and receive angle. The strongest multipath arrival may be at the start of the impulse response, at the end, or somewhere in between [10]. This effect is demonstrated in Figure 4, which illustrates a simple multipath model of an environment and its associated impulse response for two different transducer orientations. Rotating the transducer upward by 30 degrees changes the relative magnitudes of the arrivals in the channel's impulse response, resulting in the strongest arrival changing from the 2nd to the 1st multipath arrival.

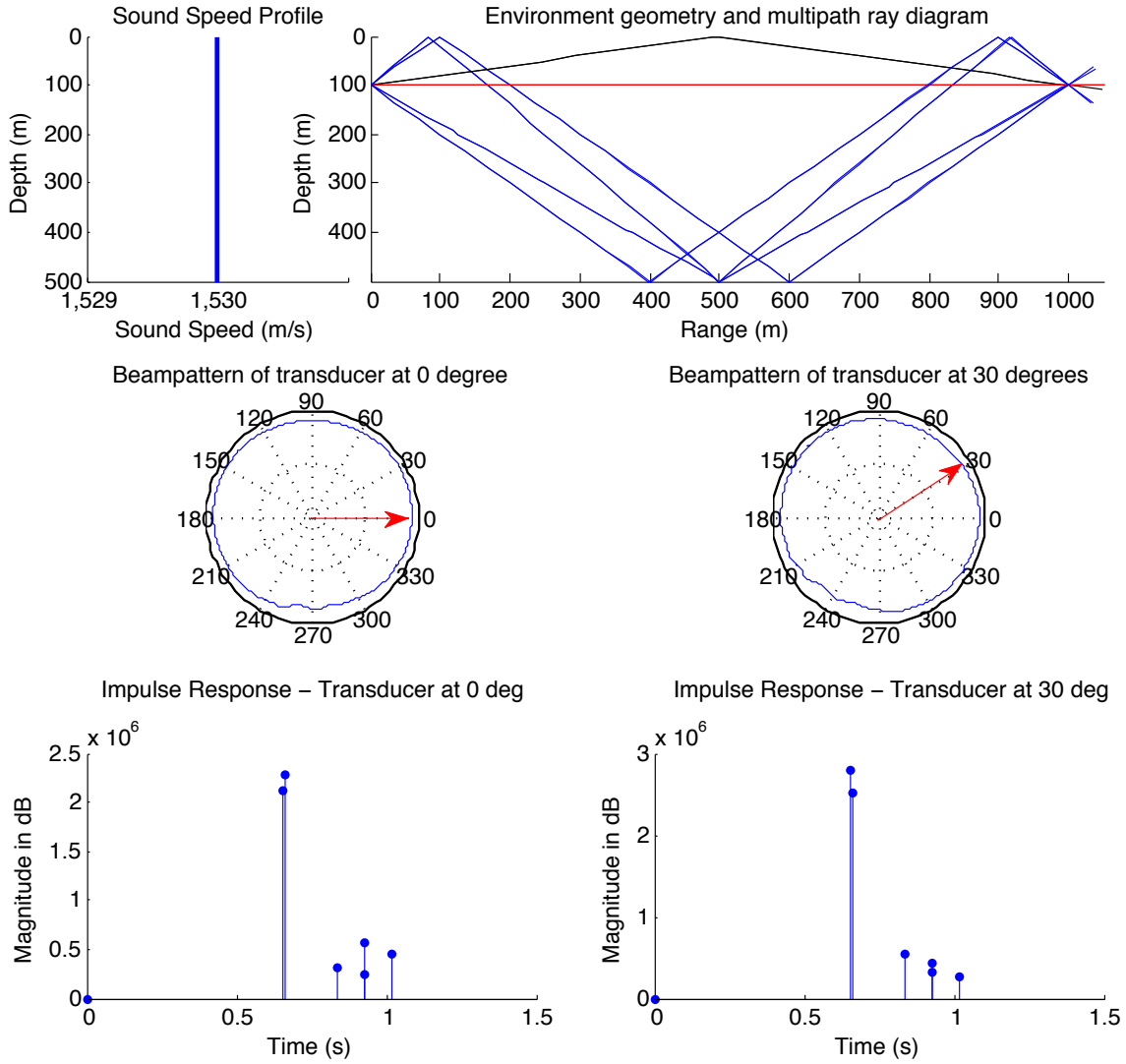


Figure 4. Variation of the impulse response caused by rotating the transducer (and beampattern). From top left to bottom right: simulated sound-speed profile (isothermal), simulated multipath of the environment, beampattern when transducer is at 0 degrees, beampattern when transducer is at 30 degrees, impulse response at 0 degrees and impulse response when at 30 degrees. Note that at zero degrees, the second arrival has the strongest magnitude, and at 30 degrees, the strongest magnitude is at the first arrival.

## B. TEMPORAL VARIABILITY

In addition to transducer motion, the impulse response will vary due to motion within the environment. There are various phenomena responsible for this motion, which fall in the two following categories [9] [11].

### 1. Long-Term

Changes that occur over a long time scale usually develop at a slow rate and do not affect the signal during its propagation through the medium. Their gradual occurrence means that the system can adapt to the changes in the environment. Since some of them can be cyclic in nature, the system can be designed to predict and adapt to these fluctuations.

#### *a. Swell*

The effect of swell is dominantly indirect, as it causes the motion of the transducers and affects the impulse response in many ways as explained in Section A of this chapter. It can also directly affect the signal reflected at the surface, inducing a Doppler effect on the signal frequencies based on the direction, speed and amplitude of the swell.

#### *b. Current*

Spatially, currents change the sound-speed profile of the water column. Temporally, the change in speed of the propagation medium intrinsically affects the speed of propagation of the signal. This change of speed induces a Doppler effect on the signal frequencies. The current creates "scintillations" (amplitude instabilities), due to the emergence of local turbulence in the current stream.

#### *c. Internal Waves*

These waves have similar effect as the current. Their inherent movement induces a Doppler effect on the signal frequencies.

#### *d. Tides*

Their period of half a day makes the change of tides to the environment relatively slow. They only affect communication channels located in or near a shallow-water area, where they modify the geometry of the multipath propagation within the medium.

### *e. Daily and Seasonal Temperature Variations*

Temperature variations such as the development of a warm surface layer affect the sound-speed profile of the water column. Again, their rate of change is very slow and does not affect the instantaneous characteristics of the communication channel.

## 2. Short-Term

Short-term variability is expressed in many different ways, which is the reason there is no consensus on a statistical characterization of the underwater acoustic channel [9]. Wind energy is the dominant cause of short-term instability. Its highly dynamic nature leaves little time for the system to adapt and can often result in the outage of the communication channel.

### *a. Surface Wave*

The ever-moving shape of the ocean surface consistently changes the geometry of the surface reflection, affecting the delays of the impulse response. From Snell's law, each wave crest forms an acoustic mirror with its own characteristic shape and focusing properties [12]. As shown in Figure 5, this change in geometry can also create caustics resulting in signal amplitudes much greater than those of the direct arrival path. The resulting impulse response can vary in time in such a manner that there is no clearly defined strongest arrival [9].

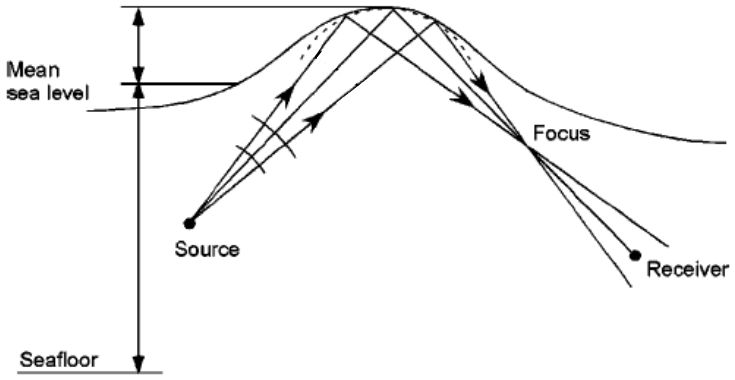


Figure 5. Qualitative description of acoustic focusing by surface wave (from [12]).

The movement of the wave will also, as in the case of swells, imprint a Doppler effect on the signal frequencies.

#### *b. Bubbles*

Air bubbles created and suspended at the air-water interface result in a significant attenuation of surface scattered signals, especially at higher signal frequencies. The "roughness" of the sea-surface breaking waves is directly related to the amount of bubbles trapped in the water [13].

#### *c. Others*

There is a long list of diverse occurrences that can cause time variability and affect the impulse response in similar ways as explained previously. Examples of such occurrence are: wakes of passing ships, fish shoals, bubble screens due to rain showers, a fresh-water front due to river discharge, etc [10]. These examples are often site-specific and neglected when designing an underwater communication system.

## C. MEASUREMENT NOISE

Measurement noise is a problem that exists in and affects practically every communication channel. However, interference due to noise can induce errors in the reception of a transmitted signal which potentially leads to errors in measuring propagation time-delays used in clock-synchronization protocols. Indeed, successful communications requires a link margin related to the signal-to-noise ratio at the receiving node. Like any sonar system, the variability of clock synchronization can be analyzed with the sonar equation.

## D. CHANNEL MODELING AND SOUNDING

Effective single model representations of the salient propagation characteristics of the underwater environment have been elusive [9]. Ocean environment modeling is still an extremely active field of research where many aspects of its physics are still not fully understood. Nevertheless, the recent advances in computer processing power have made

it possible to better simulate the communication channel. These simulations are based on various models, which are not always valid for a real environment.

In the absence of a fit-for-all underwater statistical model, channel soundings are a good alternative to the lack of prediction capability. They are measurements of the time-varying impulse response of a propagation medium [10] and replace general assumptions about the channel. A series of pulses is sent through the channel at a set interval. The receiver analyzes the received series and estimates the local channel characteristics from it. This procedure is an additional support cost to the system, but the result may greatly improve its overall efficiency.

THIS PAGE INTENTIONALLY LEFT BLANK

# IV. PROPOSED CLOCK SYNCHRONIZATION ALGORITHMS

The following algorithms account for time variability in the underwater communication channel when synchronizing the clock of slave node A to reference master node B. As stated in the introduction, this approach is based on the TSHL protocol, which is explained in the following section. Our approach relaxes the assumption in TSHL of a stable propagation delay between the synchronizing nodes. Instead, we repeatedly measure the response of the channel over a period of time and statistically describe the communication channel to better determine the propagation delay and its skew.

Our model keeps the two-stage approach developed by TSHL, but the stages are implemented differently to accommodate for their respective timing message signaling approaches (one-way message dissemination and two-way message exchange). The following sections describe the original TSHL protocol in more detail followed by an explanation of how our approach extends each of the protocol's stages to account for a communication channel characterized by a time-varying response.

## A. TSHL ACOUSTIC NETWORK PROTOCOL

The TSHL clock synchronization protocol [1] is one of the first developed and published and was specifically designed for underwater or high-latency sensor networks. Its main feature is to split the clock synchronization process into two distinct stages based on the importance of correcting the skew of a clock before its offset. By first correcting the skew of the clock, the offset is converted from a variable function of time to a constant. This is necessary because otherwise the high latency of the channel makes it impossible to precisely correct the local clock since its offset will already have changed by the time the correction is applied.

In the first stage, the skew of the clock is determined using a one-way dissemination method. A series of chirps ( $x_1, x_2, x_i, ..., x_n$ ) is sent from reference node B at a known and constant reference pulse interval (RPI) to the synchronizing node A. Linear regression based on a least–squares fit [14] is performed on the measured

synchronization pulse interval (SPI), which is the time interval between the arrival time of the pulses ( $y_1, y_2, y_i, ..., y_n$ ), relative to the known RPI. The resulting slope $f_A$ of this line represents the clock skew of node A. This one-way exchange of pulses is illustrated in Figure 6. The first stage is independent of the propagation delay which is assumed to be constant for the short time duration when the series of chirps is transmitted.

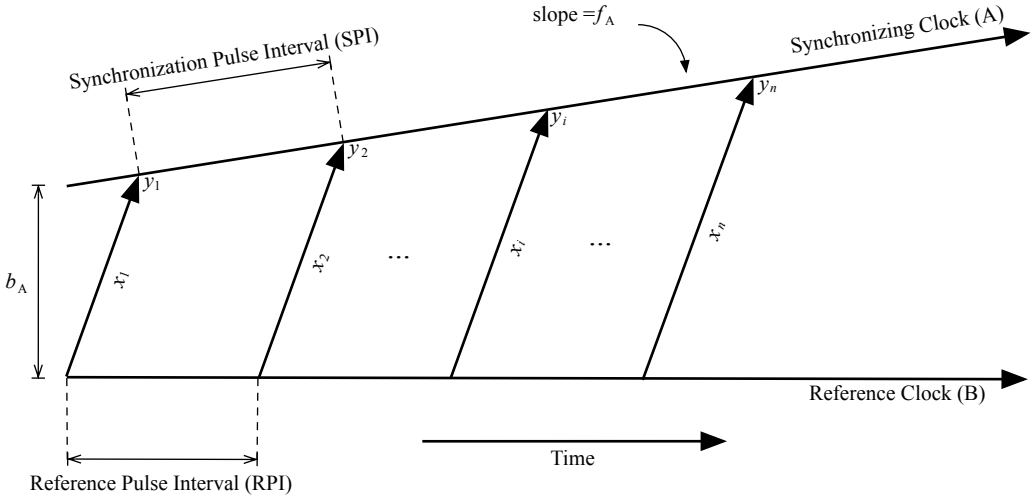


Figure 6. One-way dissemination method used in the first phase of the TSHL protocol to correct the skew of the local clock A compared to the reference clock B.

When stage one is completed, the skew $f_A$ between the node's clocks has been determined, and $b_A$ is the only remaining unknown value in Equation 1. The known skew can be corrected such that clock A's time-line, illustrated in Figure 6, is now parallel to the reference clock line (horizontal). At this point, the offset $b_A$ changes from being a time-dependent variable to a constant since the distance between the two lines remains the same.

This constant offset is corrected using a two-way exchange methodology. As shown in Figure 3 and assuming a constant bi-directional propagation delay, a set of messages is exchanged from node A to B and then from B to A. The respective node records and generates time-stamps, using its own clock, when the messages are transmitted ($T_1$ and $T_3$) and received ($T_2$ and $T_4$). This timing information is compiled

by the synchronizing node, where the total propagation time of the two messages will be $P$ from Equation 2. Under the assumption that the channel is reciprocal, the one-way propagation time delay $p_k$, where $k$ is the message number, is obtained from the average of the two messages

$$\frac{(T_4 - T_1) - (T_3 - T_2)}{2} = p_k. \tag{5}$$

Knowing the one-way propagation delay from Equation 5, where $p_k = p$, we can use Equations 3 or 4 to determine the clock offset $b_A$. Both equations should yield the same value for the offset $b_A$.

Eventually, various external instabilities (listed in Chapter II) will affect the oscillating frequency of one or both nodes, changing the skew difference between their local system clocks thus requiring a repeat of the clock-synchronization protocol.

## B. STAGE 1: CHANNEL SOUNDING AND SKEW CORRECTION

Our approach to the skew correction looks deeper into the physical attributes of the received chirps. When subject to a multipath environment, an acoustic modem will "pick" an arrival or path in accordance to a pre-defined metric. In the case of the Teledyne Benthos acoustic modems, the most energetic path or largest peak is selected as the synchronizing reference datum. As explained in Chapter III, this reference arrival can temporally change within the impulse response of a time-varying communication channel. Such an environment will influence the arrivals within the impulse response differently, resulting in some arrivals being more stable over a period of time than others. The following model essentially changes the pre-defined synchronization metric used by the acoustic modem. The new metric is based on the structure of the impulse response estimated by sending a series of chirps through the channel (channel sounding).

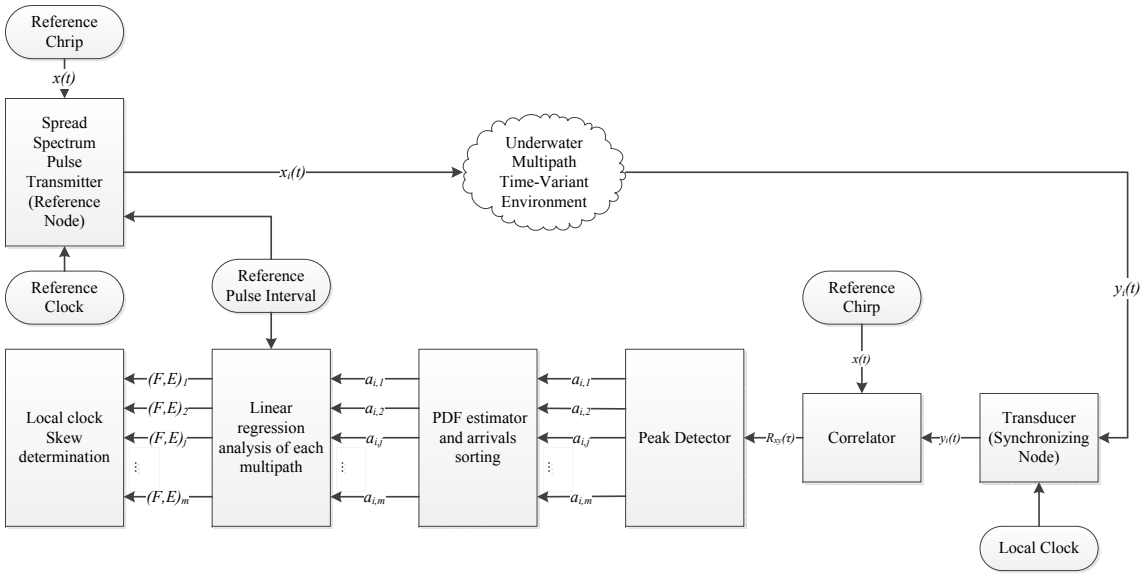


Figure 7. Skew determination system diagram illustrating the transmission of the $i^{th}$ chirp of n transmitted. The response of every chirp is collected and recorded by the peak detector where the analysis of the ensemble begins, resulting in the determination of the skew of the local clock.

The block-diagram of the proposed system is illustrated in Figure 7.

The starting point of the process is the generation by the reference node B of a digital impulse train, ultimately based on its clock frequency. The length of this impulse train must be sufficient to provide enough chirps to the synchronization node A for the linear regression algorithm. Results from [1] indicate that the empirical rule of thumb for the optimal number of impulses required to calculate the skew is 25. The selection of the RPI must be based on the sampling frequency of the system and the intended measurement precision of the skew. The length of the whole impulse train must be such that there are enough samples to cover the scale of the clock skew.

The characteristics of the pulse affect how accurately each multipath arrival can be distinguished from one another within the impulse response. Since the function of the algorithm is essentially the same as channel sounding, reference [10] identifies linear frequency-modulated (LFM) chirp trains and pseudorandom (PRN) binary sequences as the most suitable types of probe signals. A key attribute of LFM and PRN waveforms is their use of a wide spectral bandwidth. Another factor contributing to the resolution of

the arrivals is the length of each chirp by virtue of the large time and bandwidth product of the probe signal. A longer chirp helps identifying the pulse within a noisy environment but depending on the spread of the impulse response, a long pulse can also introduce some superposition in the sense that successive pulses in time cannot be distinguished from each other. The multipath structure and distance between the two synchronizing nodes determines the delay spread of the impulse response and is, therefore, linked to establishing the length of the pulse signal.

As the series of chirps is created, it is mixed to the carrier frequency and transmitted as the $i^{\text{th}}$ chirp ( $x_i(t)$ ) of $n$ total chirps by the reference node's transducer. The environment affects the transmitted signal $x_i(t)$, as explained in Chapter III. The received signal is then denoted as $y_i(t)$ in Figure 7.

The signal $y_i(t)$ received by the synchronizing node's transducer is filtered, mixed back down to baseband, and digitized based on the sampling frequency regulated by the node's local clock.

The time delay between a signal recorded at two spatially separated sensors can be recovered using a correlator, even in the presence of noise [15]. In this system, the known reference pulse $x_i(t)$ is correlated with the signal received by the synchronizing node $y_i(t)$ to produce $R_{xy_i}(\tau)$. The distance between the peaks in $R_{xy_i}(\tau)$ represent the time delays between the multiple copies of the transmitted pulse. These originate from the multipath characteristic of the channel. $R_{xy_i}(\tau)$ can also be used to estimate the channel impulse response at time $t$.

The peak detector then applies a threshold to detect the location of the peaks present in the signal $R_{xy_i}(\tau)$. These peaks represent the signal propagation time difference between the different paths present in the channel at time $t$.

Each arrival time is noted in Figure 7 as $a_{i,j}$ which refers to the $j^{\text{th}}$ received multipath arrival time from the $i^{\text{th}}$ out of $n$ transmitted pulses. The arrival times are then stored in a matrix A as illustrated in Figure 8. It is important to note that the number of

detected arrival can vary among the received chirp responses. Therefore, *m* represents the maximum number of arrivals detected in a single received pulse. The final size of matrix A is then *n* x *m*.

$$i = \text{chirp index} \left\{ \overbrace{\begin{pmatrix} a_{11} & \cdots & a_{1j} & \cdots & a_{1m} \\ \vdots & \ddots & \vdots & \iddots & \vdots \\ a_{i1} & \cdots & a_{ij} & \cdots & a_{im} \\ \vdots & \iddots & \vdots & \ddots & \vdots \\ a_{n1} & \cdots & a_{nj} & \cdots & a_{nm} \end{pmatrix}}^{j = \text{multipath arrival times}} \right. = A$$

Figure 8. *n* x m matrix A of arrival times generated by the peak detector.

The peak detector will not necessarily detect the same number of arrivals for each received pulse. As explained in Chapter III, the time variability of the channel impulse response can affect the energy level received from a particular multipath and prevent it from being detected by the peak detector. Therefore, the detected arrival times present in a single column of Figure 8 do not necessarily represent the same multipath arrival for each one of the received responses. The arrivals of each multipath must, therefore, be properly grouped before the skew can be found. To do so, a sorting algorithm aligns each multipath in a single column of a matrix, keeping the received detected arrival for a particular pulse on the same row.

To determine the main multipath arrivals, a probability density function (PDF) is estimated using all of the detected arrival in matrix A of Figure 8. The time indexes of the peaks of this PDF are extracted and used to represent the main multipath, identified individually by the index $q$ in Figure 9, of the channel where $q = 1,2,...,Q$. The maximum number of multipaths identified by the algorithm can be pre-set. In Figure 9, the $s$ largest peaks of the PDF will be identified as the main multipath, where $s = Q$.

Each main multipath is represented by a column in a new matrix B, an example of which is illustrated in Figure 9. The time indexes are compared with the detected arrival time of each pulse. If a detected arrival time corresponds to one of the determined main multipath arrival times, it is transferred to the new matrix on the respective row of the

pulse from which it was detected and the column to which multipath it is associated. If no arrivals are detected, a zero is inserted in the matrix as a place holder. The size of matrix B can be different from the size of A, depending on how much the impulse response of the channel varies between the transmission times of the *n* pulses.

$$i = \text{chirp index} \left\{ \overbrace{\begin{pmatrix} a_{11} & 0 & \cdots & a_{1q} & \cdots & a_{1(s-1)} & a_{1s} \\ \vdots & \vdots & \ddots & \vdots & \iddots & \vdots & \vdots \\ a_{i1} & a_{i2} & \cdots & a_{iq} & \cdots & 0 & a_{is} \\ \vdots & \vdots & \iddots & \vdots & \ddots & \vdots & \vdots \\ a_{n1} & a_{n2} & \cdots & a_{nq} & \cdots & a_{n(s-1)} & a_{ns} \end{pmatrix}}^{j = \text{multipath arrival index}} \right\} = B$$

Figure 9. Example of matrix B generated by the PDF estimator and arrival sorting algorithm. B is the matrix of sorted arrival times. The number of rows in B remains the same as the number of rows in A (Figure 8) but the number of columns in B can change depending on the number of multipath arrivals identified by the algorithm. Zeros are inserted where no arrivals can be correlated to an identified multipath within a received pulse.

Now aligned, each common ensemble of arrivals (individual columns of matrix B in Figure 9) is processed by a linear-regression algorithm. As mentioned in Section A of this chapter, the estimated time delay measured for each chirp for a common multipath arrival and the known RPI can be used to perform a linear-regression analysis. A straight line is fit to the data in each of the columns of B. This analysis results in two values: $F_j$ is the slope of the best fit line and $E_j$ represents the goodness of fit of this line, better defined as the linear correlation coefficient [14]. As before, the slope $F_j$ represents the skew between the synchronizing and reference clocks. The linear correlation coefficient $E_j$ is used in the next step of the algorithm to select the most stable multipath arrival.

The final step of the process identifies which set of arrivals is the most stable and reliable within the series of chirp responses analyzed. This decision is based on the calculated value of $E_j$ and the number of arrivals detected in a particular set. The linear correlation coefficient is calculated based on the standard deviations of the measured and expected time delays and their associated mutual covariance [14]. The value of the

mutual coherence can vary between 0 and 1, where 1 represents the best possible fit (i.e., all the points are on the line) and 0 the worst possible fit (no correlation among the arrivals of the ensemble).

Time variability within a specific multipath causes the arrivals to vary in the time domain, resulting in a greater deviation of the arrivals from the best-of-fit line. We sort all of the correlation coefficients $E_j \; j = 1,2,...,m$ and find the largest one. This most stable multipath arrival is chosen to be the one with the highest correlation coefficient (i.e., closest to 1), and this arrival has the least deviation from its best-of-fit line.

Another metric required to confirm this most stable multipath arrival is the number of arrivals included in the ensemble. A low number of arrivals within a multipath arrival ensemble is a good indication by itself that it is not a reliable multipath arrival (if a column of B contains several zeros). As well, it can negatively influence the result of the linear regression. As an example, performing linear regression with only two arrivals produces a perfect correlation coefficient of 1. The most stable multipath is identified by the number of multipath detections and the associated time-variability of that multipath. The user must make this judgment.

## C. STAGE 2: OFFSET CORRECTION

Our approach to correct the offset $b_{\mathrm{A}}$ (as defined in Equation 1) of the skew-corrected clock compared to a reference is different than THSL's as it does not assume that the propagation between the two nodes is the same as shown in Figure 3. The reason channel reciprocity is not a valid assumption in the underwater environment is explained in Chapters II and III. Such a situation is illustrated in Figure 10 by separately labeling the one-way propagation delays.

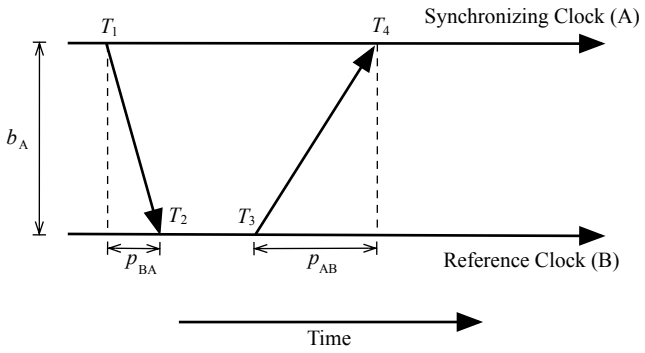


Figure 10. Two-way message exchange of timing messages between the synchronizing (A) and reference (B) nodes where the individual one-way propagation delay differs. In this example $p_{A,B} > p_{B,A}$. After [1].

The definition of $P$ in Equation 2 is modified as

$$p_{A,B} + p_{B,A} = P. \tag{6}$$

As well, Equations 3 and 4 are modified to account for the different propagation delays

$$T_2 - T_1 - p_{A,B} = b_A \tag{7}$$

$$T_4 - T_3 - p_{B,A} = -b_A. \tag{8}$$

The basis of our approach is the two-way message exchange used by most clock-synchronization protocols. Its distinction lies in its ability to differentiate the propagation delays for both one-way propagation channels instead of using an average based on the round-trip propagation time. A chirp is sent ahead of each message allowing the chirp response of the one-way communication channel to be determined by the receiver. Both estimated impulse responses are correlated at the synchronizing node A to determine the difference in propagation delay $\Delta p$ between the two of them. This delay $\Delta p$ is the difference between the time corresponding to the largest peak and zero lag. This method can be used because the modem always synchronizes on the largest amplitude arrival. The offset of the clock can be calculated using this propagation delay difference and the four time-stamps generated by the two-way message exchange.

An overall system diagram of this adapted two-way message exchange is presented in Figure 11 and is further explained below.

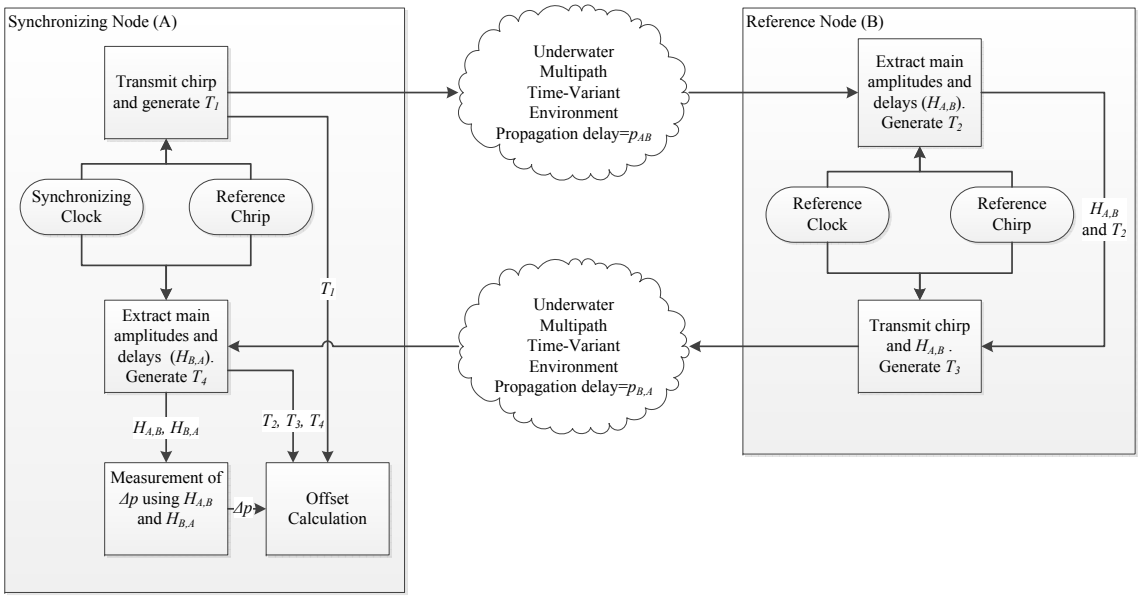


Figure 11. Adapted two-way message exchange for calculating the offset of a skew-corrected local clock compared to a reference.

The synchronizing node A starts the offset correction process by sending a new pulse ahead of the offset calculation request message to reference node B. The time of the start of the transmission is time-stamped $T_1$ and recorded by node A.

As it propagates through the channel, the pulse is transformed as explained in Chapter III. The yet-to-be-determined propagation delay is denoted as $p_{\mathrm{A,B}}$ in Figure 11. Time-stamp $T_2$ is recorded by the receiver upon first detecting the arrival of the pulse sent by node A. From the pulse response, the instantaneous one-way impulse response from node A to B is determined using a matched filter and identifying the peaks of the resulting time-series. This impulse response is required later in the algorithm at the synchronizing node. To reduce the bandwidth required to send it across the channel for processing, the estimated impulse response is compressed by retaining its main characteristics, which are the amplitudes of the largest peaks and their associated time indices. These characteristics are represented as $H_{\mathrm{A,B}}$ in Figure 11.

The reference node then sends the same new reference pulse before transmitting the second message of the exchange. Time-stamp $T_3$ is recorded concurrently to the beginning of the transmission of the second message. It carries the two time-stamps generated by node B, $T_2$ and $T_3$, as well as the compressed impulse response information $H_{\mathrm{A,B}}$ recorded from the probe signal preceding the first message.

The second message propagates through the channel from node B to A. The message is transformed by the channel as discussed in Chapter III. The yet to be determined propagation delay is denoted as $p_{\mathrm{B,A}}$ in Figure 11. Time-stamp $T_4$ is generated by the receiver upon detecting the arrival of the chirp sent by node B. From this received chirp, the instantaneous one-way impulse response from node B to A ($H_{\mathrm{B,A}}$) is estimated and its information compressed using the same process explained in step 3 of this algorithm. From their respective recorded characteristics, the main arrivals of both estimated impulse responses are reconstructed in the time-domain from $H_{\mathrm{A,B}}$ and $H_{\mathrm{B,A}}$. Their cross-correlation allows for the time-delay estimation between the two signals. Based on the assumption that the modem will synchronize with the strongest arrival, the difference in propagation delay $\Delta p$ (Equation 9) will be the time index difference between the highest peak of the cross-correlation and its zero lag:

$$p_{\mathrm{A,B}} - p_{\mathrm{B,A}} = \Delta p = \tau^{*}. \tag{9}$$

The total propagation delay $P$ of both messages and the time-delay difference $\Delta p$ can be combined to evaluate one of the two propagation delays ($p_{\mathrm{B,A}}$ or $p_{\mathrm{A,B}}$). Adding Equations 6 and 9 together, we get

$$P + \Delta p = 2\, p_{\mathrm{A,B}}. \tag{10}$$

The one-way propagation delay $p_{\mathrm{A,B}}$ can be determined from Equation 10:

$$\frac{P + \Delta p}{2} = p_{\mathrm{A,B}}. \tag{11}$$

The second propagation delay (in this case $p_{\mathrm{B,A}}$) can be evaluated from

$$P - p_{A,B} = p_{B,A}. \tag{12}$$

Either one of the one-way propagation delay can be used in Equation 11 as $\Delta p$ can be positive or negative. Whichever one-way propagation is evaluated in Equation 11, the remaining one can be determined using Equation 12.

The last step of the algorithm consists of evaluating the offset $b_A$ between the two nodes' clock using Equations 7 or 8. The result of both equations should be the same.

## D. TIME REVERSAL APPROACH

A time reversal approach was investigated as a way to evaluate the individual one-way propagation delays of the two-way message exchanged methodology. This approach initially appeared very promising since one of its benefits is the elimination of the multipath effect of the communication medium. However, one of the assumptions of time-reversal is the requirement of reciprocity within the channel [16]. The basis of our algorithm is the existence of different one-way propagation delays resulting in a non-reciprocal channel. Therefore, a time reversal approach was rejected for our problem.

# V. COMPUTER SIMULATIONS STUDIES

We implemented the approach described in Chapter IV in Matlab. The Bellhop and VirTEX underwater acoustic propagation models (both compatible with Matlab) are used to simulate a simple underwater acoustic communication channel. The aim of the simulation is to prove our conceptual approach prior to conducting an in-water experiment. The environmental models, the simulated environment's parameters, the step-wise results, and the clock-correction stages (skew and offset) are explained in the following sections.

## A. BELLHOP

Bellhop [17] is a ray-tracing program developed by Michael B. Porter and distributed as part of the Acoustic Toolbox software package. Based on ray theory, it can produce two-dimensional acoustic ray tracing for a given channel geometry and underwater environment. Various options can be selected and inputs given to the model to better define the environment and provide more realistic simulation. Once the channel geometry and environment are defined, Bellhop provides various graphical and numerical outputs.

## B. VIRTEX

The VirTEX family of algorithms was designed by Peterson and Porter [18]. The algorithms build on the results obtained by a Bellhop simulation and add the effects of multipath and Doppler introduced by environmental motion. The algorithm computes the time series that would be observed at a hypothetical receiver location.

## C. DESCRIPTION OF THE SIMULATED ENVIRONMENT

Our simulation environment is very simple. The aim of our simulation is not to model a specific environment but to test the theory of our algorithm. The environment, illustrated in Figure 12, consists of a transmitter and a receiver, both situated at a depth of 100 m and separated by a distance of 1 km. The sound-speed profile is isothermal for simplicity. Time variability is introduced in the environment by randomly changing two

parameters: the orientation of the transmitter and the phase of a simulated wave on the sea surface. As explained in Chapter III, the orientation of the beam pattern can change the path which has the most energy. As well, surface waves can alter the delay-spread characteristics of the impulse response. The surface wave is modeled as a sinusoidal wave with phase randomly changed throughout the simulation to provide a non-stationary surface boundary.

Normally, both nodes of the system will operate with the same sampling frequency. To simulate a skew difference between the two clocks, the sampling frequency of the synchronizing node is slightly altered when recording the incoming chirp time-series. This artificial method creates a known skew between the two nodes' clocks. For this simulation, the sampling frequency at the receiver is reduced from 48,000 samples/sec to 47,885 samples/sec. This reduction in sampling frequency results in a skew of 417 ppm.

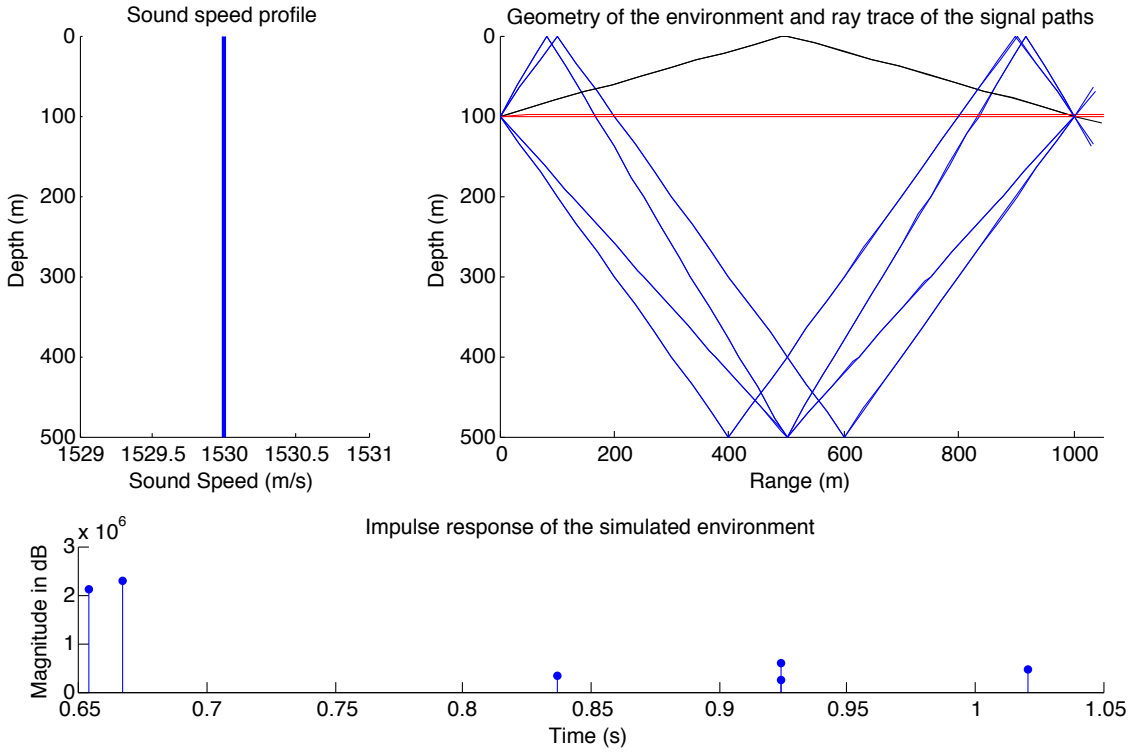


Figure 12. Characteristics of the simulated environment. From the top left corner: the sound-speed profile; the geometry of the environment and its associated ray paths; the impulse response of the communication channel.

## D. STEP-BY-STEP SIMULATION RESULTS

This section presents the formal results of the simulations. Figures illustrating the different stages of the algorithm are also presented to help visualize some of the explanations from Chapter IV.

### 1. Phase 1: Skew Correction

A 5-ms LFM chirp based on a 5-kHz bandwidth is created and designated as the reference chirp. The chirp is sent through the channel 20 times at a RPI of one per second. The orientation of the transmitter and phase of the surface wave is randomly changed prior to each transmission and remains the same during the transmission of a single chirp. The simulation is run with and without a skew difference.

The receiver, knowing the sampling frequency, RPI and number of pulses sent, separates the pulses into a matrix of 20 chirps as illustrated in Figure 13.

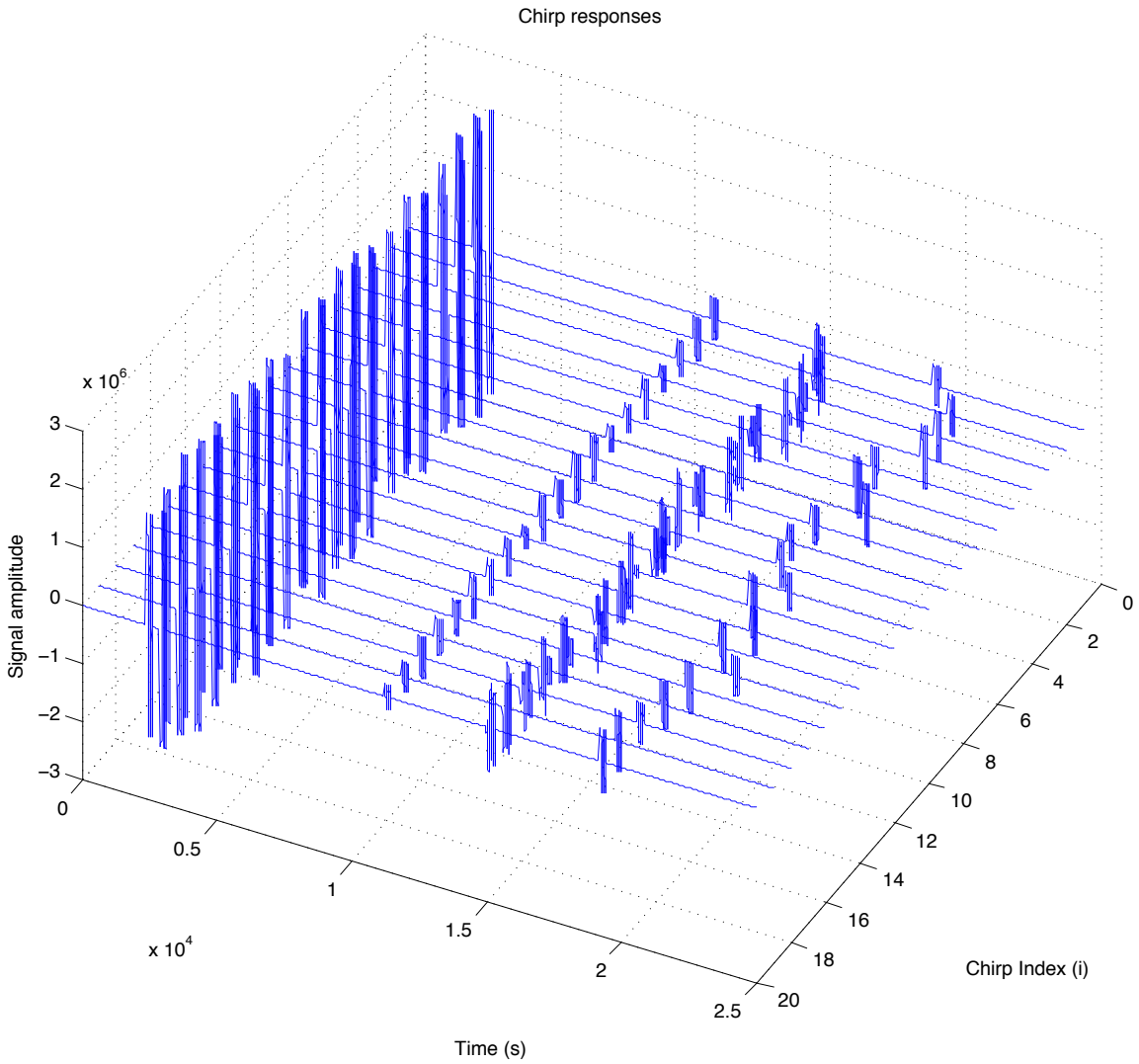


Figure 13. Ensemble of 20 chirp responses with no clock skew.

Without any signal processing, time variability is already noticeable in Figure 13. Let $n$ denote the number of probing pulses (chirps) used in any given experiment. $n = 20$ is then the number of measurement waveforms displayed in Figure 13. We denote these $n$ waveforms by $\{y_i(t)\}_{i=1}^{n}$.

We compute the cross correlation $R_{xy_i}(\tau)$ between the reference chirp $x(t)$ and each of the measurement signals $y_i(t)$ to create the ensemble of cross correlations $\{R_{xy_i}(\tau)\}_{i=1}^{n}$ plotted in Figure 14.

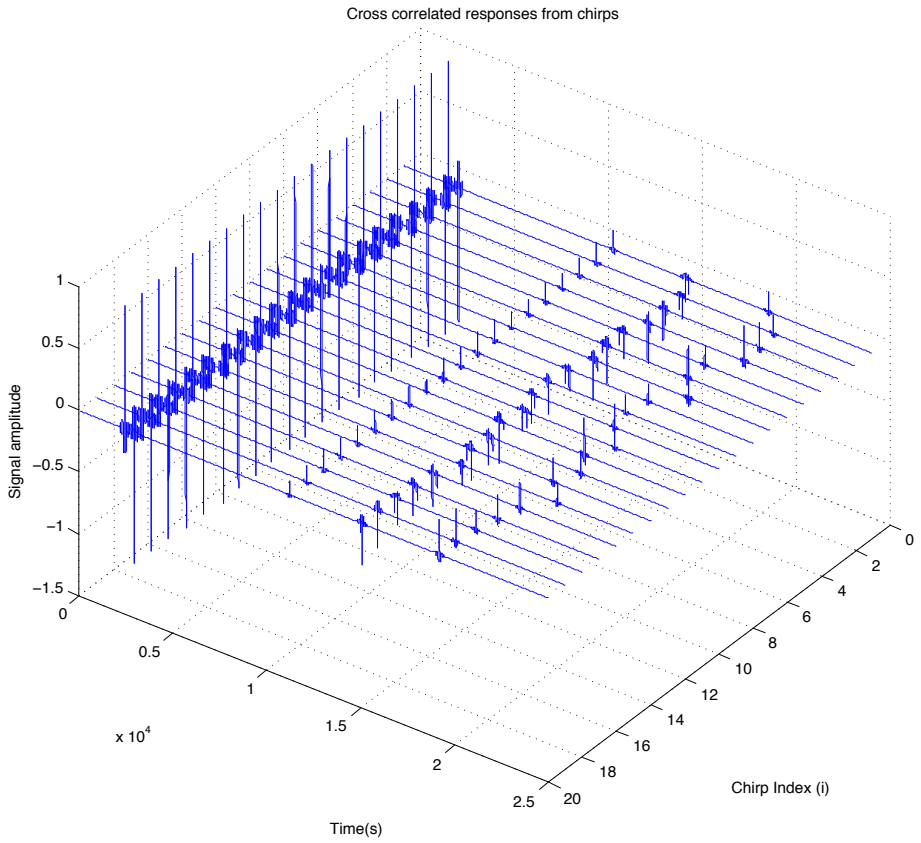


Figure 14. Ensemble of 20 cross-correlated received chirp responses with no clock skew present.

Note that the signals in Figures 13 and 14 contain $m = 5$ multipath arrivals that make up the chirp response. Let $j$ denote the "arrival index," or the index on the $m$ multipath arrivals $\{a_j\}_{j=1}^{m}$ that occur in a given single measurement waveform, $j = 1, 2, \ldots, m$ .

The peaks displayed in Figure 15 are estimated from the cross-correlation signals displayed in Figure 14. First, the individual arrivals in the cross-correlation waveforms are selected to be the multipath arrivals that exceed a small threshold chosen by the user. For each of the arrivals in a given correlation waveform $R_{xy_i}(\tau)$, we find the time $\tau^*$ corresponding to the time at which a peak occurs by choosing the time lag $\tau^*$ such that $R_{xy_i}(\tau^*) = \max\{R_{xy_i}(\tau)\}$.

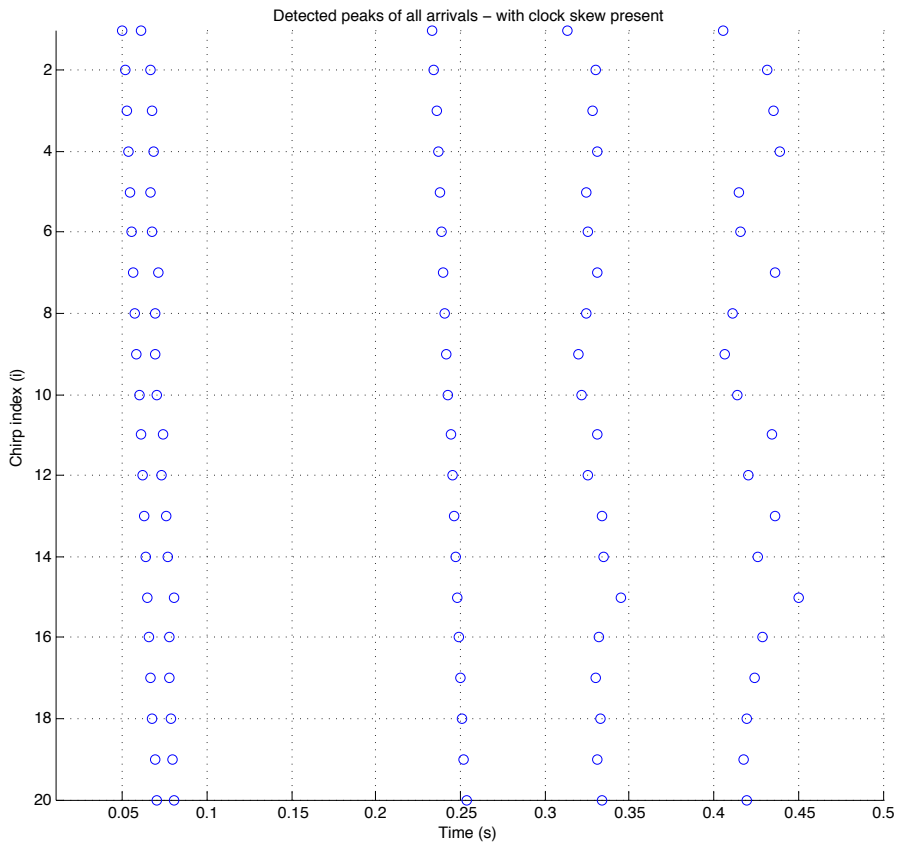


Figure 15. The peak times for an experiment in which clock skew is present: The peak times $u_{ji}$ derived from the ensemble of $n = 20$ measurement signals depicted in Figure 14 are plotted in this figure. Note that each of the $m = 5$ arrival wavelets $a_j, j = 1, 2, \ldots, m$ has a corresponding ensemble $U_j = \{u_{ji}\}_{i=1}^{n}, j = 1, 2, \ldots, m$ associated with it.

We see in Figure 14 the ensemble of $n$ waveforms and in Figure 15 the ensemble of peaks of waveforms that result from the $n = 20$ probing pulses from the transmitter. After peak detection, we see in Figures 15 and 16 that each multipath arrival has a corresponding ensemble of $n = 20$ peaks associated with it. The peak arrival times shift over time due to the skew between the transmitter and receiver clocks. An example of an ensemble of waveforms with zero skew is depicted in Figure 16.

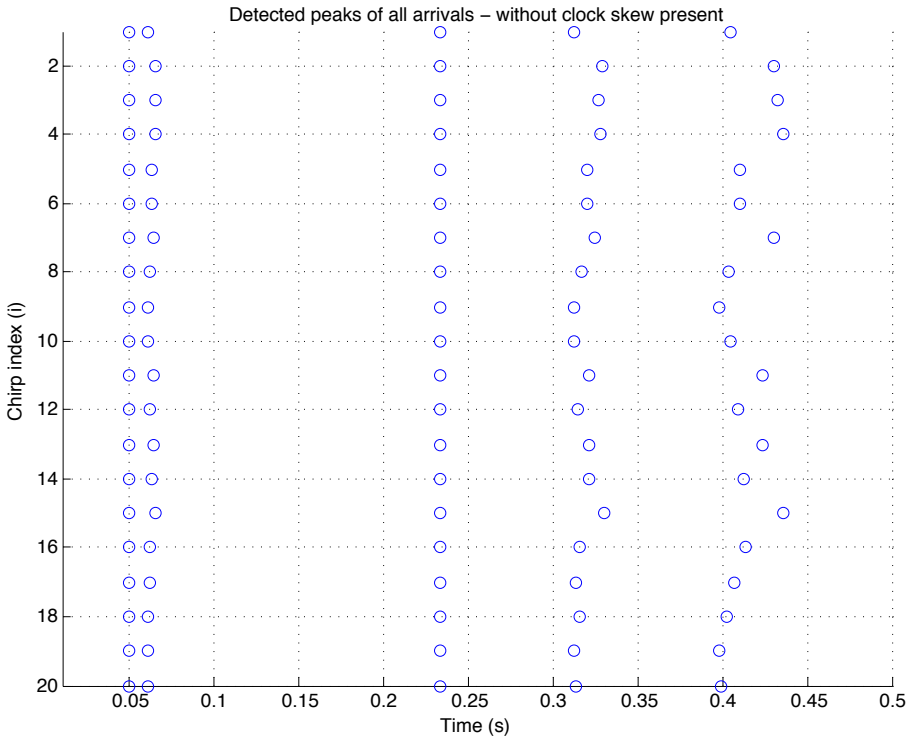


Figure 16. The peak times for an experiment in which zero clock skew is present: The peak times $u_{ji}$ derived from the ensemble of $n = 20$ measurement signals depicted in Figure 14 are plotted in this figure. Note that each of the $m = 5$ arrival wavelets $a_j, j = 1, 2, \ldots, m$ has a corresponding ensemble $U_j = \{u_{ji}\}_{i=1}^{n}, j = 1, 2, \ldots, m$ associated with it.

Let $i$ denote the peak index corresponding to each of the $n$ peaks that occur for a single multipath arrival in a given ensemble constructed from the data displayed in Figures 15 and 16. Because $n$ probe pulses create an ensemble of $n$ waveforms, there are $n$ peaks in an ensemble corresponding to the $j^{\text{th}}$ multipath arrival in Figures 15 and 16, $i = 1, 2, \ldots, n$. We denote the $i^{\text{th}}$ peak time for the $j^{\text{th}}$ multipath arrival by $u_{ji}$. We denote the ensemble of peak times for the $j^{\text{th}}$ multipath arrival by $U_j = \{u_{ji}\}_{i=1}^{n}$, $j = 1, 2, \ldots, m$.

For each multipath arrival $a_j, j = 1, 2, \ldots, m$, we estimate a PDF of peak arrival times using the ensemble $U_j = \{u_{ji}\}_{i=1}^{n}, j = 1, 2, \ldots, m$. We use a kernel density estimator

with a Gaussian kernel to build the PDF estimates [19]. Once all $m$ PDFs are estimated individually, we plot them on a single graph as depicted in Figure 17. We see that in Figures 15, 16 and 17 there are $m = 5$ multipath arrivals.

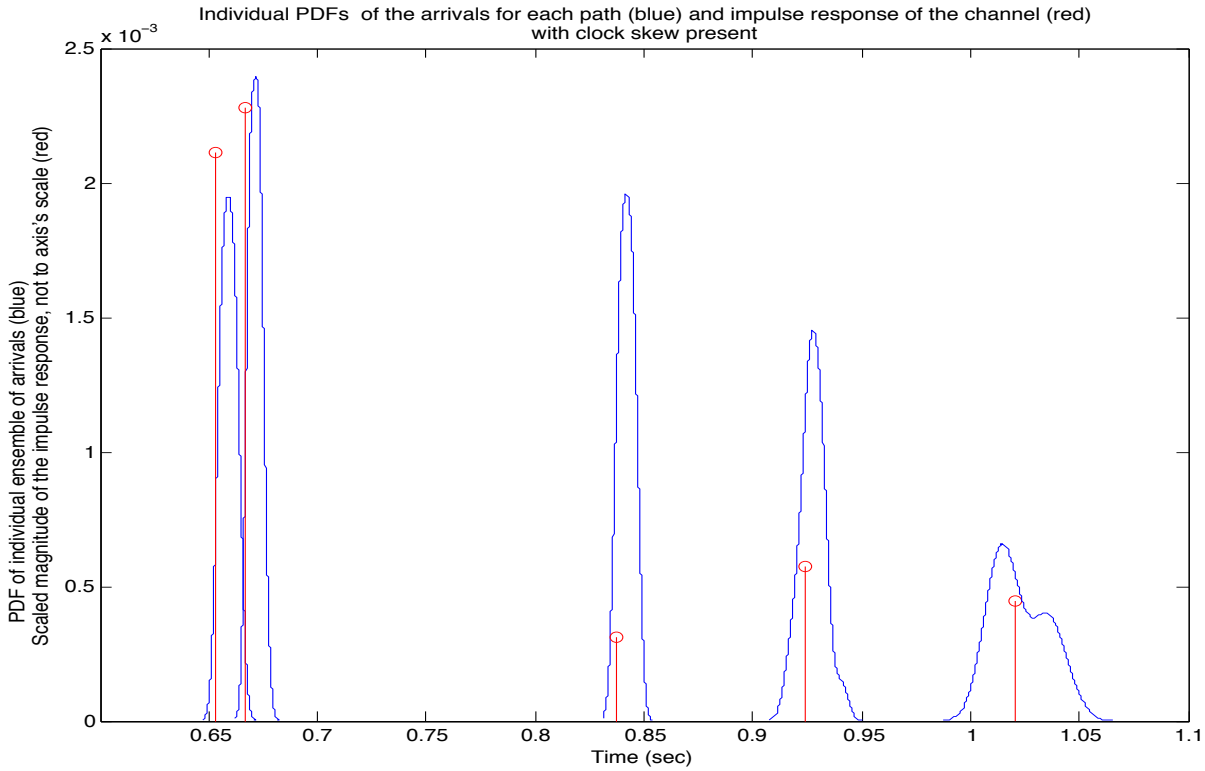


Figure 17. The scaled simulated impulse response (a set of Kronecker delta functions) of the channel is plotted in red. The estimated PDFs of the individual arrival wavelets are plotted on a single graph and appear in blue. Note that the delta functions occur at the times at which the chirp pulses begin, so the centers of the PDF estimates are shifted slightly to the right of delta functions.

The shape of each PDF, as illustrated in Figure 17, is representative of the stability of each signal propagation path. The direct paths and bottom-bounce paths are not affected by the time variability of the environment, which is only present at the water surface interface. These unaffected paths are characterized by sharp and narrow PDFs whereas the surface-bounce paths are wide and low. To demonstrate the time-variability of the environment, the non-Doppler affected estimated impulse response, as shown in Figure 12, is superimposed on Figure 17. It is important to note that the amplitudes of

the PDFs are not related to the amount of energy propagated through the associated path. The third arrival shown in Figure 17 is a good example of the case in which the weakest signal path is very stable.

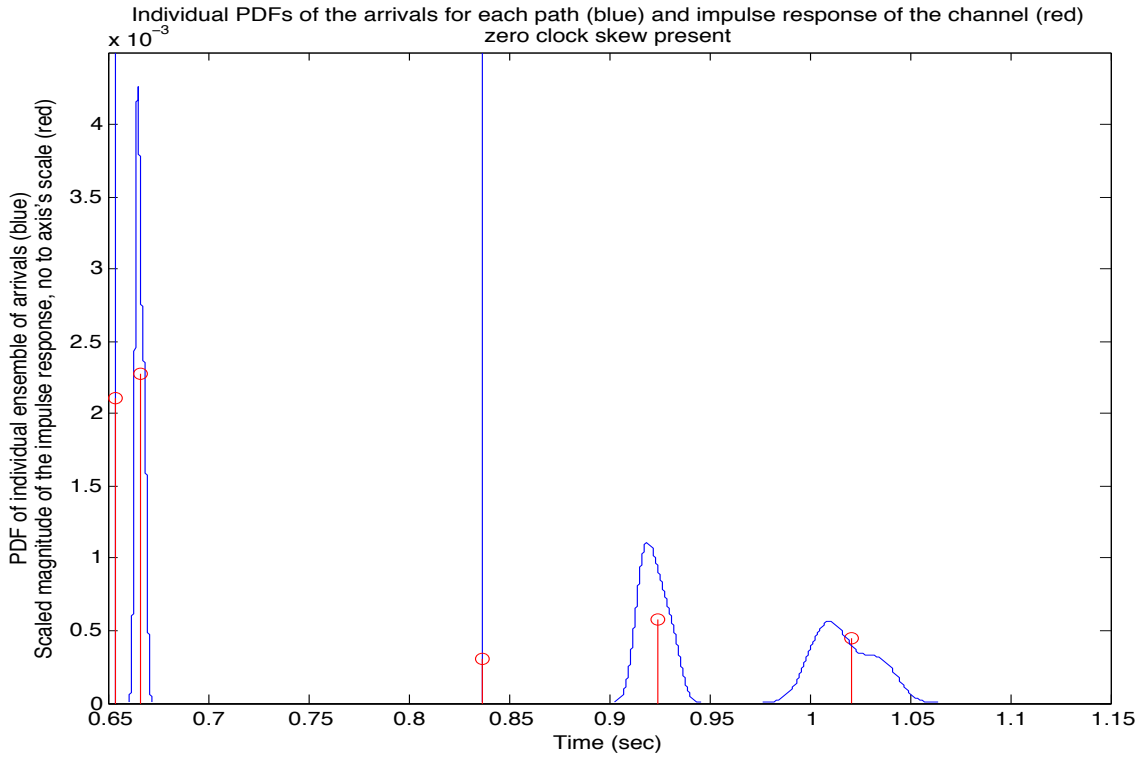


Figure 18. The scaled simulated impulse response (a set of Kronecker delta functions) of the channel is plotted in red. The estimated PDFs of the individual arrival wavelets are plotted on a single graph and appear in blue. Note that the delta functions now occur in the middle of the chirp pulses, as zero skew is present.

Figure 18 is a replica of Figure 17 but with zero skew present. Since the 1st and 3rd arrivals are not affected by the time variability of the channel and zero skew is present, their respective PDFs are now represented by Kronecker delta functions. In contrast to Figure 17, the delta functions now occur in the middle of the chirp pulses.

A least-squares linear regression algorithm is applied to each ensemble of arrivals. The result of this linear regression is the clock skew difference $F_j$, from which the coefficient of determination $E_j$ can be calculated as explained in Chapter IV. Since the tolerance of a clock is usually measured in ppm, Equation 13 can be used to convert the skew to $Fp_j$ to compare the measured value with the published tolerance of a clock:

$$1{,}000{,}000(F_j - 1) = Fp_j. \tag{13}$$

The simulation results for the first phase of the clock-synchronization algorithm are illustrated in Table 1. The algorithm chooses the first path as the most reliable (shaded arrival in Table 1) as it has the highest correlation coefficient (perfect in this case). This is expected, since both the first and third arrivals do not interact with the sea surface and, therefore, no time variability is introduced in their associated signal propagation path (direct and single bottom bounce) as illustrated in Figure 12.

Table 1. Skew correction simulation results. The shaded result corresponds to the most stable arrival set as selected by the algorithm (the set with the largest correlation coefficient).

| Simulation and set clock skew | Arrival Ensemble ($U_j$) | Skew ($F_j$) | Correlation coefficient ($E_j$) | Skew in ppm ($Fp_j$) |
|---|---|---|---|---|
| #1 No clock skew (0 ppm) | 1 | 1.000000000000000 | 1.000000000000000 | 0 |
| | 2 | 1.000087954260652 | 0.999999926902282 | 88 |
| | 3 | 1.000000000000000 | 1.000000000000000 | 0 |
| | 4 | 1.000289301378446 | 0.999999011969708 | 289 |
| | 5 | 1.000683255012531 | 0.999995976887908 | 683 |
| #2 With clock skew (417 ppm) | 1 | 1.000416666666667 | 1.000000000000000 | 417 |
| | 2 | 1.000504620927318 | 0.999999926963154 | 504 |
| | 3 | 1.000416666666667 | 1.000000000000000 | 417 |
| | 4 | 1.000705968045113 | 0.999999012792314 | 705 |
| | 5 | 1.001099921679198 | 0.999995980236109 | 1099 |

After artificially introducing a clock skew in the simulation, the algorithm successfully determines the skew as 417 ppm, which is the value expected from the reduction in sampling frequency at the synchronizing node (48,000 samples/sec to 47,885 samples/sec).

This simulation demonstrates that time variability can affect the measurement of the skew between two clocks. The skew values calculated from the ensembles of the

multipath arrival times affected by time variability varies greatly. In the worst case (ensemble #5) the skew value in ppm is nearly three times the real skew value.

### 2. Stage 2: Offset Correction

The same environment and reference chirp as in stage 1 are used to simulate our approach to the clock-offset correction. The simulation is designed to follow the steps explained in Chapter IV and illustrated in Figure 11. It focuses on the calculation of the difference $\Delta p$ in propagation time between the two messages sent in the two-way timing message scheme. Once this parameter is determined, the other unknown values ($P, p_{A,B}, p_{B,A}$ and $b_A$) can be found using the four recorded time-stamps and Equations 2, 11 and 12. An example of how these parameters can be calculated with these equations is illustrated in Figure 19.

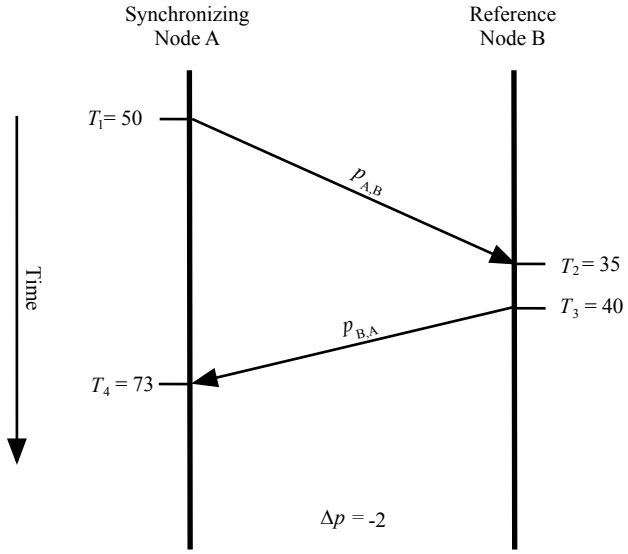


Figure 19. Example of time-stamp exchange to determine the clock offset $b_A$ between nodes A and B.

From Equation 2, the total propagation time $P$ is calculated as

$$(T_4 - T_1) - (T_3 - T_2) = (63 - 50) - (40 - 35) = 18 = P. \quad (14)$$

Then, using Equation 11, and knowing $P$ and $\Delta p$, we get

$$\frac{P-\Delta p}{2}=\frac{18-(-2)}{2}=10=p_{\mathrm{A,B}}. \tag{15}$$

The last propagation delay $p_{\mathrm{B,A}}$ can be calculated from

$$P-p_{\mathrm{A,B}}=18-10=8=p_{\mathrm{B,A}}. \tag{16}$$

Finally the offset $b_{\mathrm{A}}$ can be determined using either Equations 7 or 8.

To test our approach, the simulation must create an environment where a $\Delta p$ will exist between the two message propagation delays. Assuming that the modem (node) picks the strongest arrival to synchronize with, we see that the simulation must vary the location of this arrival within the impulse response of the two message transmissions to create a $\Delta p$. The parameters used in Figure 4, where the transmitter was tilted from 0 to 30 degrees, were used again for this simulation since they illustrate the desired temporal displacement of the strongest arrival. The steps of the simulation, illustrating the various signal processing steps, are described in this section.

The synchronizing node A initializes the clock offset correction phase following the determination of the clock skew in stage 1. It sends a reference chirp and an offset correction request message to the reference node B while also creating and storing a time stamp $T_1$ when the transmission is initiated.

The received chirp response, illustrated in Figure 20, is processed, where its main characteristics (peak amplitudes and corresponding time index) are extracted in order to limit the amount of information transmitted across the channel. Time stamps $T_2$ and $T_3$ are respectively created by the reference node when it receives the first message and transmits the second one. The difference between these two time stamps represents the processing or handling of the request by the reference node. The reference node compiles the two time-stamps and the characteristics of the analyzed estimated impulse response into a message, which is sent back to the synchronizing node following the transmission of another chirp.

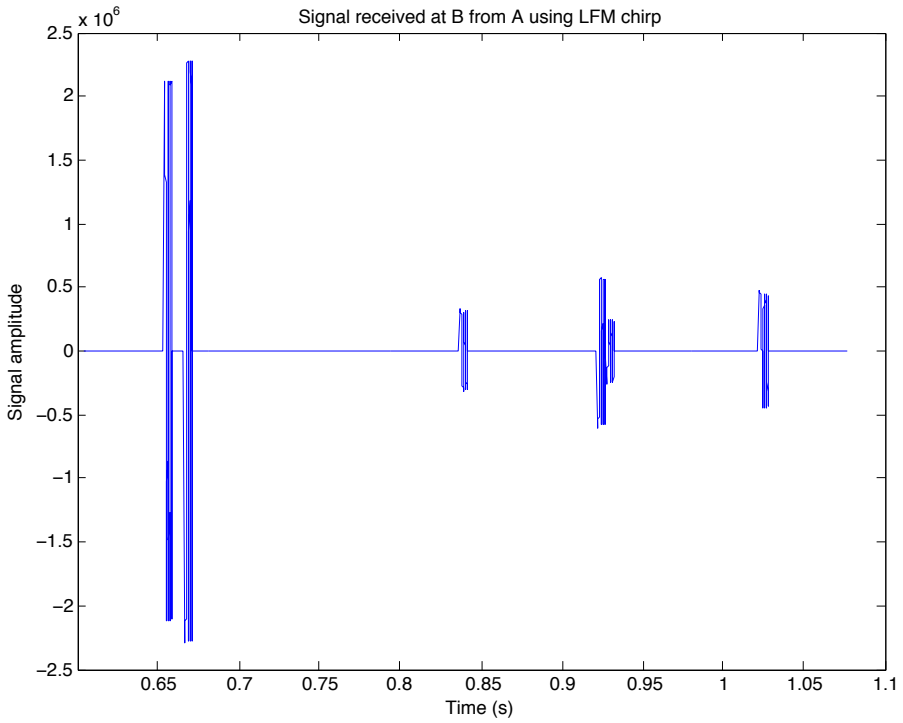


Figure 20. LFM chirp response received by the reference node B.

The synchronizing node receives the chirp response and processes it in the same manner as did the reference node. This results in a basic estimated impulse response for each one-way transmission between the two nodes, illustrated in Figure 21.

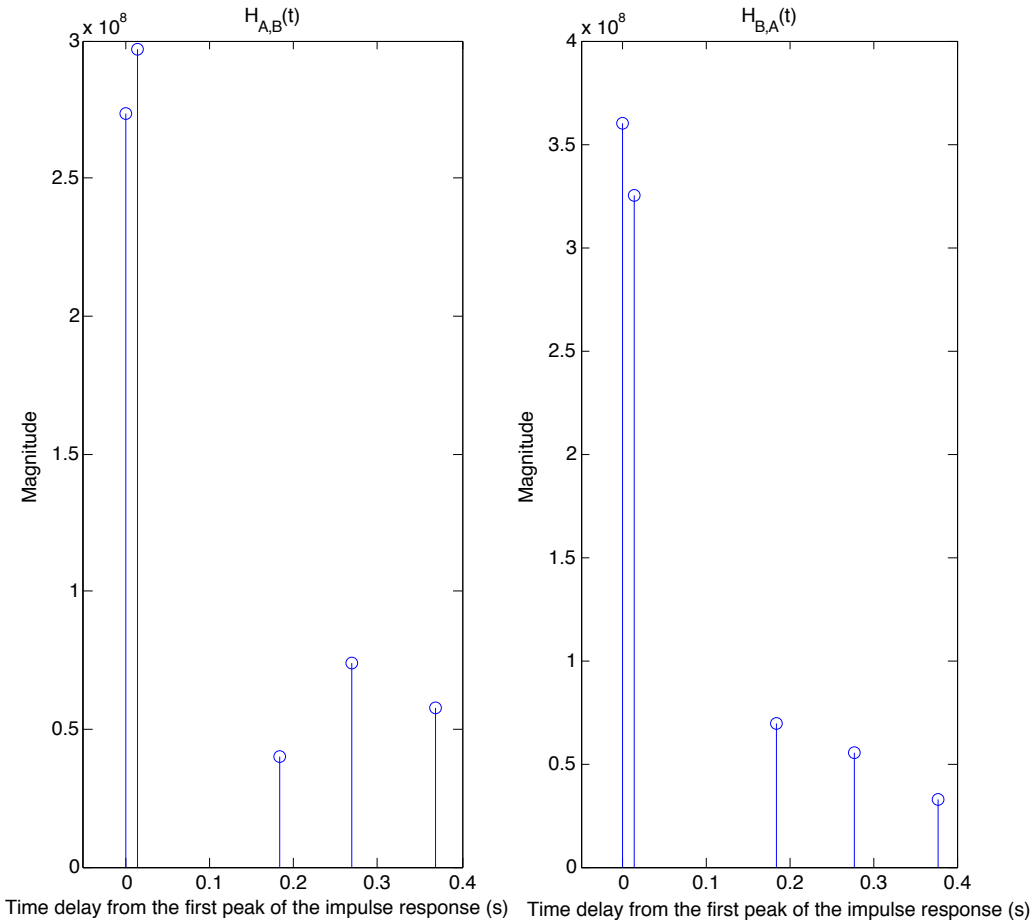


Figure 21. Simplified estimated impulse responses from the two transmissions

These two estimated impulse responses are cross-correlated resulting in the cross correlation signal plotted in Figure 22.

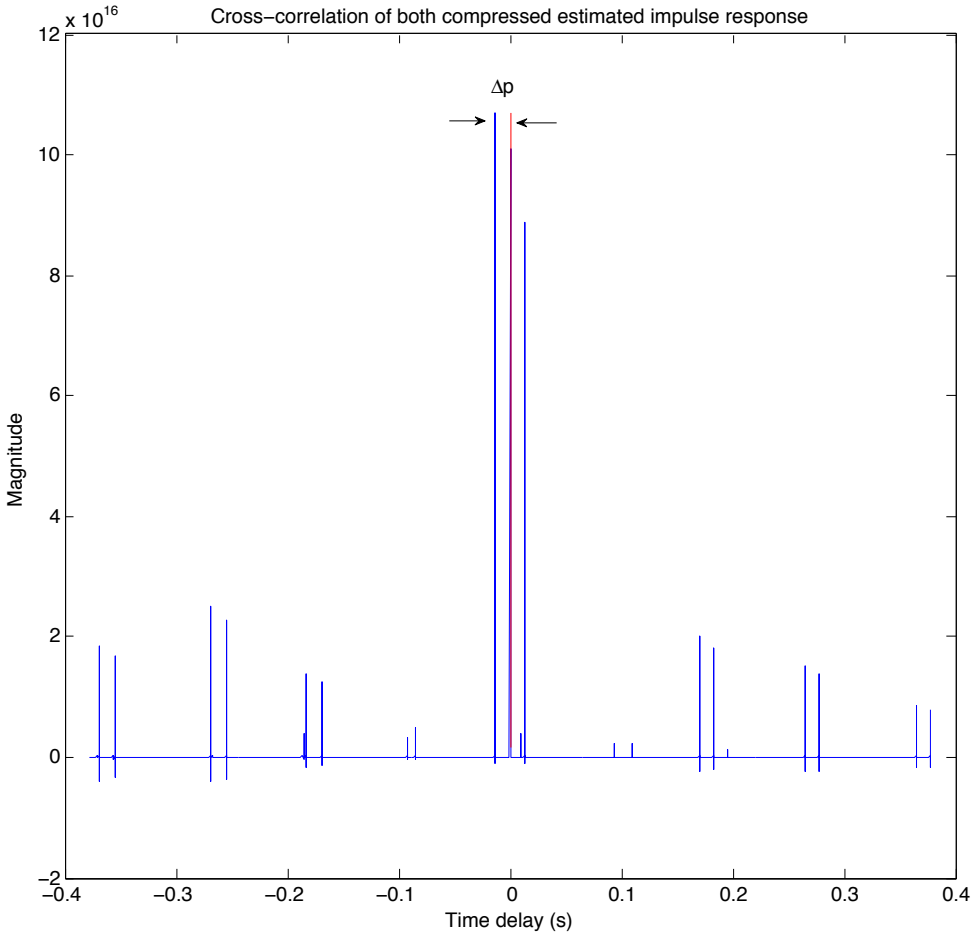


Figure 22. Cross-correlation of both simplified impulse responses. The red line indicates the middle of the cross-correlation. The distance between the highest peak and the middle of the cross-correlation represents $\Delta p$ .

The delay between the highest peak and the center of the cross-correlation (time index 0) is the difference in propagation delay $\Delta p$ between the two messages sent. The measured time series simulated by VirTEX is referenced in the time domain to the beginning of the transmission, as shown in Figure 20, which allows the determination of the "true" propagation delays $p_{\mathrm{B,A}}$ , $p_{\mathrm{A,B}}$ and $\Delta p$ using Equation 9.

Table 2. True and calculated values of the difference in propagation delays between the two messages during the two-way exchange.

| | |
|---|---|
| True $p_{A,B}$ | 0.6664 sec |
| True $p_{B,A}$ | 0.6536 sec |
| True $\Delta p$ | -0.0128 sec |
| Measured $\Delta p$ from cross-correlation | -0.0128 sec |

As stated at the beginning of this section, once $\Delta p$ is determined, the clock offset is easily calculated. The simulation proves the theory of our approach since it successfully and precisely determines the difference in propagation delays and clock offset.

# VI. DEL MONTE LAKE EXPERIMENT

## A. OBJECTIVE

The aim of the experiment is to test and prove the algorithms described in Chapter IV in an actual, time-variant, underwater environment. Only the first stage (skew correction) is tested during the experiment. The second stage requires resources not available to this project, such as access to the firmware of the Teledyne Benthos acoustic modems.

Del Monte Lake, situated on the campus of the Naval Postgraduate School is selected for its accessibility and minimal environmental studies requirements and approvals. The general concept of the experiment consists of transmitting and recording a series of chirps between two acoustic modems. The recorded data are downloaded from an on-board digital recorder and processed separately. During the post-experiment processing, the arrivals of chirp responses are tracked and processed to determine the skew difference between the clocks of the two acoustic modems (nodes). The lake environment on the day of the experiment, the equipment used, the test procedures, selection of parameters and an evaluation of the results are explained in more detail in the following section.

## B. ENVIRONMENTAL DESCRIPTION

The experiment was conducted during the afternoon of 2 May 2012 on the Del Monte lake. A satellite picture [20] of the area is illustrated in Figure 23.

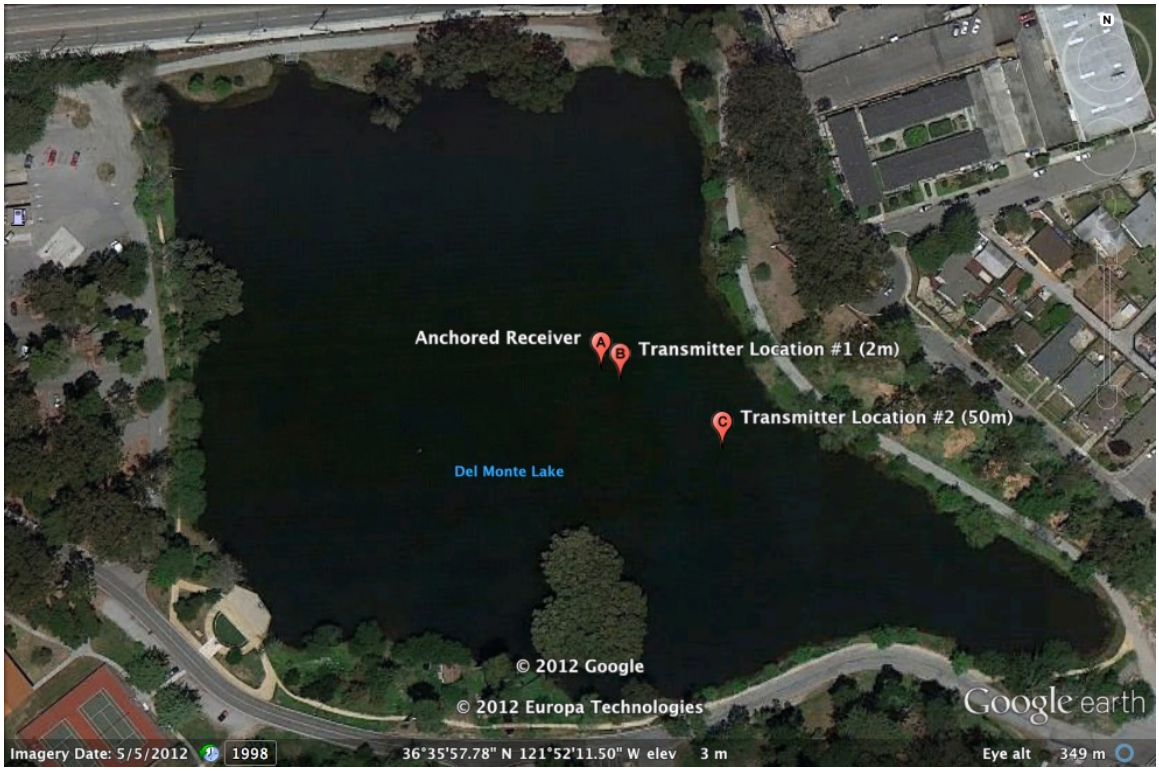


Figure 23. Satellite picture of Del Monte Lake and locations of the acoustic modems during the experiment (from [20]).

It was a warm sunny day with reported winds of 24 km/h [21]. The wind was strong enough to generate waves on the surface of the lake and made it difficult to maintain a stationary location with the small aluminium boat. From a previous experiment on the lake, the depth of the water was found to be approximately 2 m over most of the lake. The bottom of the lake consists of thick mud. The water temperature was not measured but was assumed to be isothermal through the water column due to the very shallow depth. The water fountain (not shown on Figure 23) was turned off to reduce the amount of noise present in the lake.

## C. EQUIPMENT DESCRIPTION

### 1. Aluminum Boat and Motor

A 13 foot aluminum boat equipped with a Minn Kota ENDURA Pro C2 transom-mounted trolling freshwater electric motor was used to conduct the experiment. It was

used to deploy the acoustic modem and served as a working platform on which the deck box and laptop were operated to perform the experiment.

### 2. Teledyne Benthos SM-75 SMART Modem

A Teledyne Benthos SM-75 Smart Modem Acoustic Release Technology (SMART) [5] was refurbished and fitted with an onboard digital recorder, as illustrated in Figure 24.


Figure 24. Teledyne Benthos SM-75 SMART modem (from [5]).

The modem operates in the low-frequency (LF) range of 9 -14 kHz and uses a sampling frequency of 10240 samples/sec. The digital recorder is equipped with a 4-GB Secure Digital High Capacity (SDHC) card, which records the baseband received signal by the modem in minute-long .wav or .pcm files. The gain of the received signal is continually adjusted, using an automatic gain controller (AGC), to keep the signal level constant in the recording. The AGC information is also recorded as part of the baseband signal by the digital recorder. A command is sent to the SM-75 to start and stop the digital recording, which allows the recording of selected desired events. Once recovered, the SM-75 can be dismantled and the SDHC card containing the recorded data can be removed. These recordings are then uploaded to a stand-alone computer for post-

processing and analysis. For better results, Teledyne Benthos provides a Matlab routine which uses the AGC information of a recording to restore the signal to its original level and continuity.

The LF beam pattern of the SM-75 is illustrated in Figure 25. This beam pattern is used in Chapter II to demonstrate the effect of a transducer rotation on the impulse response of the channel.

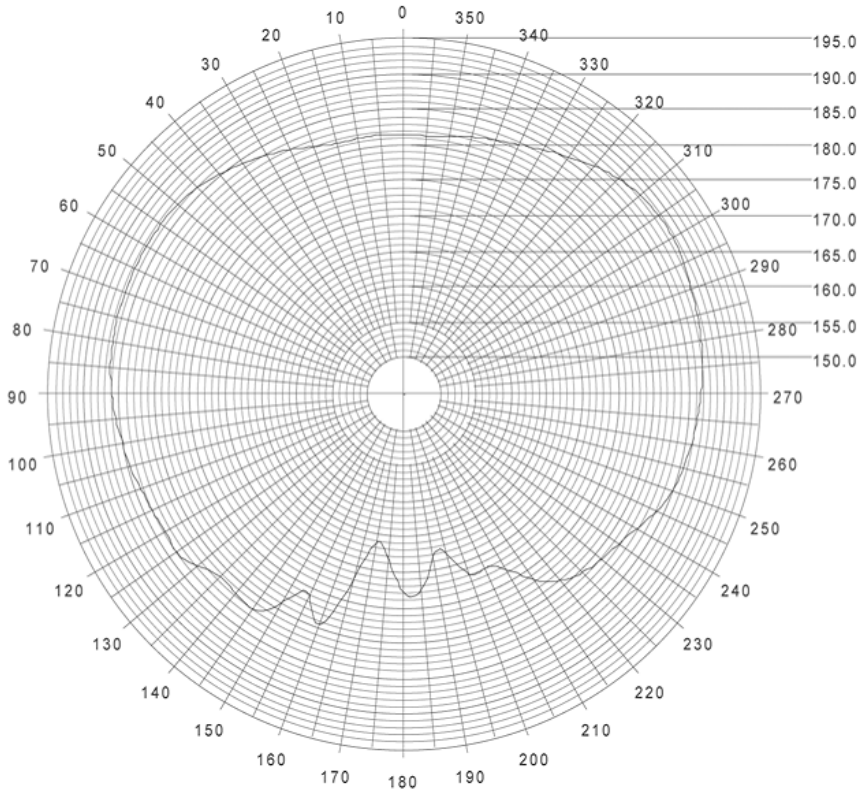


Figure 25. SM-75 LF (9-14 kHz) beam pattern (from [5]).

During the experiment the SM-75 was deployed and anchored at station A, as shown in Figure 23, at a depth of approximately 1 m. It functioned as the synchronizing node B, recording the series of chirp response transmitted by the reference node A (deck box).

### 3. UDB-9400 Universal Deck Box

As illustrated in Figure 26, the deck box is an acoustic modem where the transducer and modem electronics have been separated. Several interfaces, including a

touch screen display, are combined with the modem in a portable case, which allows a user to perform network administration within the network. The transducer is linked to the portable case via a long cable and can be deployed over the side of a boat or platform.


Figure 26. UDB-9400 Universal Deck Box, including its deployable transducer (left) (from [5]).

The modem part of the deck box uses the same communication parameters used by the SM-75 as described in the previous section. The deck box is not equipped with a digital recorder but still has a limited flash memory module, where files can be uploaded. For this experiment, .wav audio files of the various series of chirps were uploaded to the memory from which they could be played. Instead of using the touch screen to input modem commands, the deck box was connected via serial port (RS-232) to a laptop running the PROCOMM software. PROCOMM provides an easier user interface and allows the creation of script files that made the conduct of the experiment easier and faster to complete. The same laptop can also be interfaced to the SM-75 or acoustic modem.

The deck box was used as the reference node A during the experiment. Various series of chirps were transmitted at a distance of 2 m (station B on Figure 23) and 50 m (station C on Figure 23). The transducer was attached half-way down a 3 m long metal pole which was lowered and embedded in the mud at the bottom of the lake. The transducer was kept stable this way in the middle of the water depth at approximately 1 m.

## D. EXPERIMENTAL PARAMETERS

The parameters of the experiment had to be chosen to accommodate the characteristics of the test environment. Underwater acoustic modems are not normally deployed in a shallow fresh water lake and limited information was available about any previous experiments in such environments. To mitigate the risk associated with this unknown environment, various parameters were tested during the experiment. These parameters are explained in the next sections.

### 1. Distance Between the Nodes

The shallow depth of the lake makes the communication channel prone to multipath. The simultaneous arrival of many ray paths at the same time can make the retrieval of any distinct signal impossible due to temporal superposition. For a 2 m water depth, the maximum propagation delay between the direct and surface or bottom bounce paths is obtained by separating the nodes by 2 m. Assuming an isothermal water column and a constant sound of speed of 1530 m/s, the modeled time-delay difference between the two main paths is calculated to be 0.0005 s compared to 0.0001 s when the nodes are separated by 50 m. These two distances were used during the experiment. The ray paths and impulse response for nodes separated, respectively, by 2 m and 50 m were modeled using Bellhop and are shown in Figure 27.

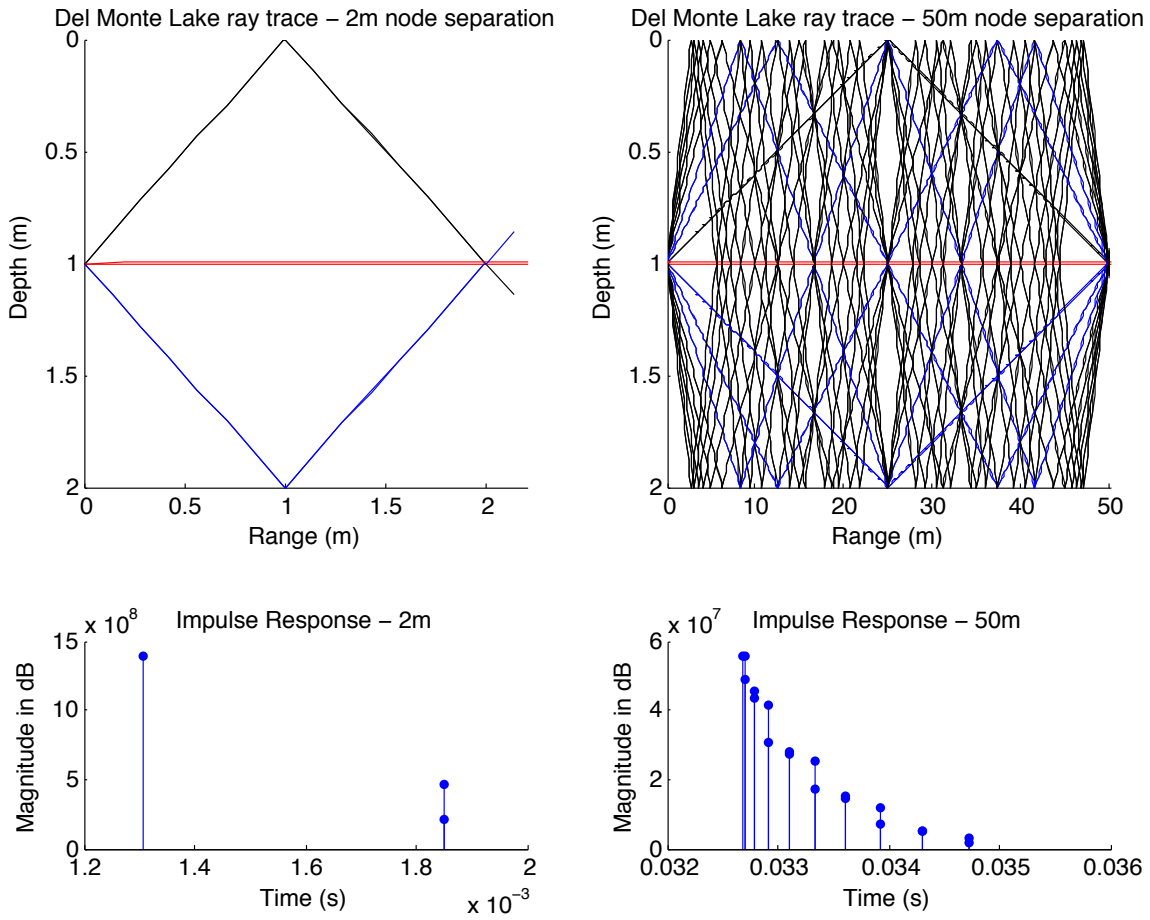


Figure 27. Bellhop model of the ray paths and impulse responses in Del Monte Lake with 2 m and 50 m node separation.

### 2. Probe Signal Characteristics

The design parameters of the probe signals are important as they determine how well each ray path can be distinguished at the receiver. It is generally accepted that the LFM chirp is a good choice as a probe signal [10]. The experiment used both LFM chirps and CW pulses in order to give some measure of the advantage of using the LFM chirp. The frequency of the chirp swept over the range of 0 to 5000 Hz which was later modulated by the modem to its operational bandwidth of 9 to 14 kHz.

The length of the probe signal affects the amount of temporal superposition at the receiver. As an example, when the nodes are separated by 2 m, the time-delay difference between the two main paths is such that a 0.5 ms probe signal will not be superimposed.

At a sampling frequency of 10240 Hz, a 0.5 ms probe signal corresponds to only 6 samples in length. Based on the fact that the ambiguity function of the chirp is inversely proportional to its length [22], a longer chirp should provide better time resolution. During the experiment, chirps of 0.5, 1, 2, 5, 10, 25 and 50 ms duration were used and compared in the post-processing analysis.

The pulse repetition interval was selected and remained at 250 ms throughout the experiment. This value was arbitrarily selected as it seemed short enough to respect the requirement to minimize the utilization of the network bandwidth when performing a clock synchronization procedure (as explained in Chapter II). Another factor that was considered was that the interval be short enough so that the AGC does not reset in-between each probe transmission.

The final parameter was the number of pulses sent in a given series. This was selected to be 30 based on the experimental result of Syed [1]. During that experiment, it was determined that 25 pulses was the optimum number of pulses before observing a diminishing benefit in increasing the number of pulses. Since Syed's experiment was conducted over the air, our number of pulses was increased to 30 to ensure that 25 of them would be received in the less favorable underwater environment.

## E. TEST PROCEDURES

The experiment was executed in three stages, which translate into the preparation, the acquisition of measurements, and the analysis. The procedures associated with each stage are described in this section.

### 1. Preparation

In preparation for the experiment the above-stated experimental parameters were chosen. A series of 30 identical pulses was generated using Matlab and then converted to a .wav file format. Each file was uploaded to the deck box's internal flash memory via the serial port using a standard laptop computer. Once loaded in the deck box's memory,

the .wav file could be played through the modem and its transducer. A PROCOMM script file was written to execute the experiment more efficiently and with fewer manual errors.

Before proceeding to the lake, an over-the-air experiment was conducted in the Seaweb Lab to confirm that the equipment worked as planned. The original script called for the digital recorder to be turned on and off between the transmission of each series of pulses, which sometimes caused the SM-75 to reboot randomly. The script was modified so that the digital recorder was turned on at the beginning of the experiment and only turned off once every series of pulses was transmitted. This solution was effective and only one measurement was lost due to a SM-75 reboot.

### 2. Experimental Measurements

The equipment was loaded into the aluminum boat and transported to the deployment stations as shown in Figure 23. The SM-75 was deployed and its location recorded using a handheld GPS. The 2-m separation between the SM-75 and the deck box transducer was confirmed by the handheld GPS and by the ranging routine included in the onboard software of the Teledyne Benthos modems. Every pre-recorded series of probe signals was transmitted twice at both the 2-m (experiment #1 and #2) and 50-m (experiment #3 and #4) stations, for a total of four experiments. No additional experiments were performed due to the drained battery of the laptop which was essential to the conduct of the experiment. The SM-75 was recovered and the equipment was returned to the Seaweb Lab. The recordings from the SM-75 were transferred to a laptop for analysis.

### 3. Post-experiment Analysis

A log file was created along with each recording by the digital recorder. The log files identify every .wav file of duration of one-minute long or less associated with it. Time-stamps were also generated by the modem's internal clock and annotated in the log marking the beginning and ending of each files. As stated earlier in this chapter, Teledyne Benthos provides a Matlab routine that reconstructs the recording based on the

log file. With this routine, each recording was processed and the original non-AGC time series were then available in a Matlab format.

Each recording contained multiple transmissions of pulse series. These series were easily identifiable, as shown in Figure 28, and were individually extracted to be processed separately.

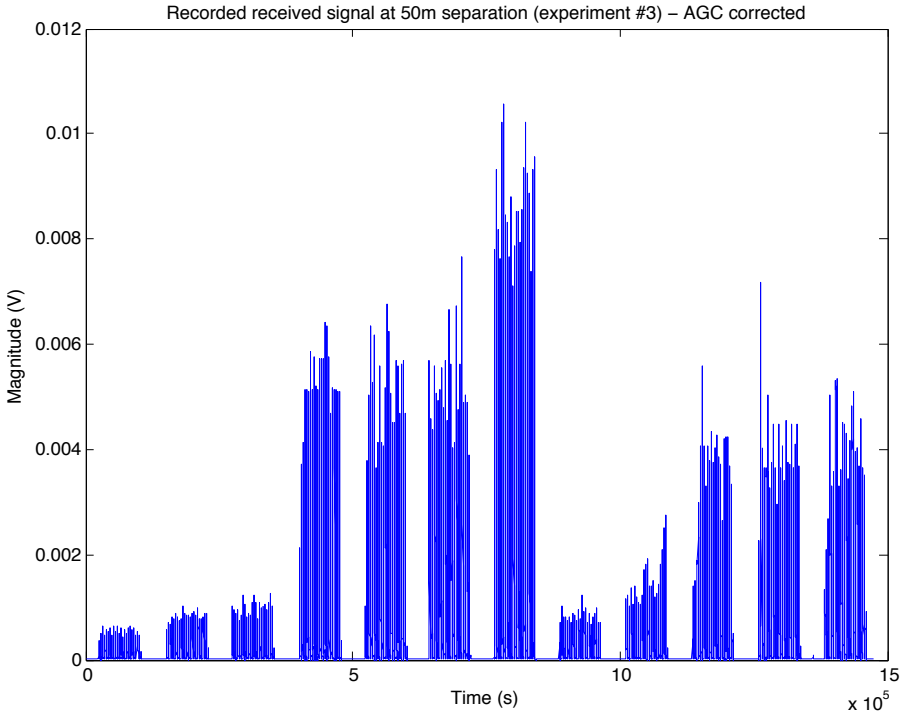


Figure 28. AGC-corrected recording where all series of probe signals were received when the nodes were separated by 50 m (experiment #3).

Each individual series of probe signals was processed separately using the same algorithms previously described in Chapter IV and V.

## F. RESULTS

The cumulative results of the analysis are illustrated in Table 3. Following Table 3, a selection of these results is expanded to demonstrate some of the noteworthy findings.

Table 3. Estimated skew (in ppm) and its related error for each different series of probe signals transmitted during each experiment. An average of the error (in ppm) for each different series of probe signals is also included.

| Estimated skew and error in ppm for each experiment (all values are in ppm) | | | | | |
|---|---|---|---|---|---|
| Probe Signal | Experiment #1 (2m) | Experiment #2 (2m) | Experiment #3 (50m) | Experiment #4 (50m) | Average Error |
| 0.5ms LFM | -42 ± 10 | -58 ± 15 | -33 ± 14 | -28 ± 6 | ±11.25 |
| 1ms LFM | -42 ± 10 | -21 ± 25 | 4 ± 16 | -55 ± 14 | ±16.25 |
| 2ms LFM | -28 ± 12 | -53 ± 17 | -45 ± 3 | -35 ± 4 | ±9 |
| 5msLFM | -38 ± 11 | -34 ± 11 | -33 ± 11 | -29 ± 4 | ±9.25 |
| 10msLFM | - | -44 ± 50 | -20 ± 14 | -28 ± 5 | ±23 |
| 25msLFM | -41 ± 14 | -54 ± 22 | -31 ± 6 | -51 ± 10 | ±13 |
| 50ms LFM | 60 ± 27 | -32 ± 27 | -34 ± 11 | 11 ± 15 | ±20 |
| 0.5ms CW | 11 ± 34 | 5 ± 46 | -56 ± 25 | -48 ± 3 | ±27 |
| 1ms CW | -46 ± 8 | 5 ± 33 | -8 ± 31 | -15 ± 15 | ±21.75 |
| 2ms CW | 70 ± 38 | -44 ± 4 | -36 ± 20 | -40 ± 27 | ±22.25 |
| 5ms CW | -42 ± 33 | 9 ± 35 | -13 ± 16 | -59 ± 21 | ±26.25 |
| 10ms CW | -30 ± 32 | -39 ± 39 | -28 ± 4 | -16 ± 26 | ±25.25 |

The digital recorder rebooted during the playing of the 10ms LFM series of pulses in experiment #1, therefore, no results are shown for this event in Table 3.

An initial glance seems to demonstrate a high variance among the results. To better analyze this variance, the uncertainty of each skew measurement is calculated [14]. The following Figures and Tables examine the source(s) of this variance and provide a higher degree of confidence in the experimental results.

From Table 3, the 2 ms LFM chirp is found to be the superior probe for this environment based on its lower average error of ±9 ppm. In Figures 29 and 30, respectively, the first 15 matched-filtered responses of the 2ms chirp when tested at 2 m (experiment #2) and 50 m (experiment #3) are shown. These figures are used as a comparison with other chirps that were identified to be less effective.

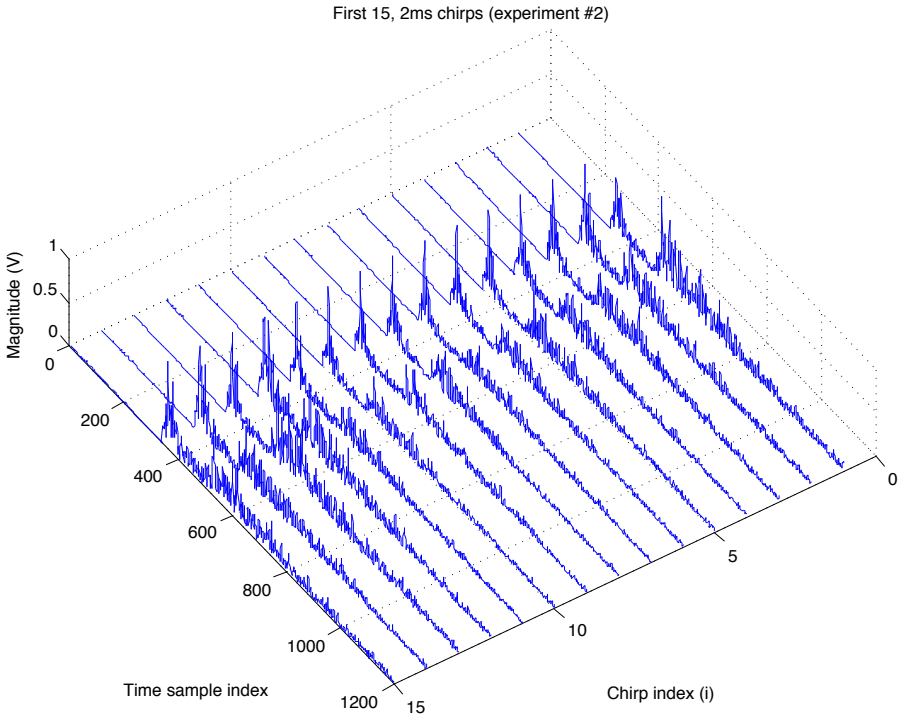


Figure 29. First fifteen 2 ms long LFM chirp responses at 2 m (experiment #2).

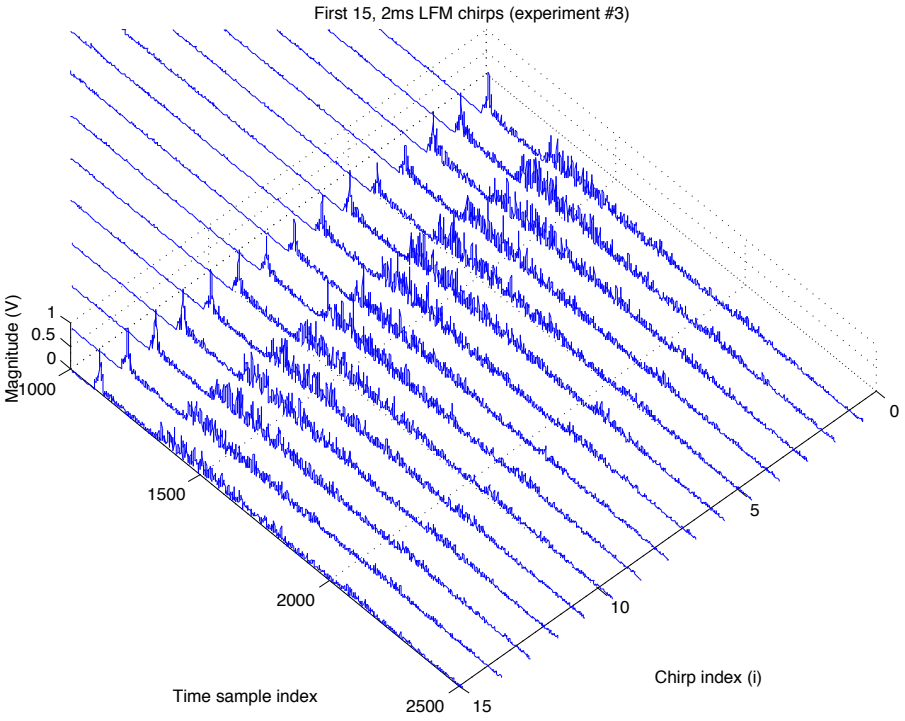


Figure 30. First fifteen 2 ms long LFM chirp responses at 50 m (experiment #3).

Looking at Figures 29 and 30, we see that the first detected and most likely the direct path is easily identifiable and looks fairly stable over the measurements. The following arrivals are not as easy to distinguish but a few peaks are estimated to be associated with a multipath arrival by the algorithm as shown in Tables 4 and 5. The data presented in these tables are the time index where a peak is detected. Performing linear regression on each of these paths allows the determination of the clock skew and its correlation coefficient, which is used to identify the most stable path. The shaded column highlights the most stable path based on its correlation coefficient. In both cases, the first path has the highest correlation coefficient, which is consistent with Figures 29 and 30. The first detected path clearly shows a slow shift of the detected peak, indicating the presence of skew between the clocks in the two nodes. Respectively following Tables 4 and 5 are Figures 31 and 32, which illustrate the same data presented in the tables. These figures clearly show the time variability of the multipath arrivals.

Table 4. Detailed results of the 2 ms LFM pulse received during experiment #2, including the correlation coefficient, clock skew (in absolute and ppm values) and its associated error.

| Analysis of 2 ms LFM pulse received during experiment #2 (2 m separation) | | | | | |
|---|---|---|---|---|---|
| Pulse Index | Time index of detected peaks for each multipath | | | | |
| | Detected path #1 | Detected path #2 | Detected path #3 | Detected path #4 | Detected path #5 |
| 1 | 362 | 389 | 530 | 557 | 599 |
| 2 | 363 | 394 | 535 | 0 | 0 |
| 3 | 363 | 389 | 540 | 566 | 600 |
| 4 | 363 | 395 | 528 | 0 | 0 |
| 5 | 363 | 0 | 531 | 0 | 611 |
| 6 | 363 | 395 | 531 | 564 | 599 |
| 7 | 363 | 390 | 535 | 565 | 599 |
| 8 | 364 | 395 | 531 | 557 | 599 |
| 9 | 364 | 390 | 532 | 564 | 602 |
| 10 | 364 | 395 | 532 | 564 | 603 |
| 11 | 364 | 395 | 532 | 559 | 0 |
| 12 | 354 | 381 | 532 | 563 | 603 |
| 13 | 364 | 395 | 532 | 0 | 0 |

| Pulse Index | Time index of detected peaks for each multipath | | | | |
|---|---|---|---|---|---|
| | Detected path #1 | Detected path #2 | Detected path #3 | Detected path #4 | Detected path #5 |
| 14 | 361 | 393 | 532 | 562 | 589 |
| 15 | 364 | 396 | 532 | 566 | 593 |
| 16 | 364 | 390 | 532 | 0 | 0 |
| 17 | 365 | 396 | 532 | 566 | 600 |
| 18 | 364 | 395 | 533 | 0 | 609 |
| 19 | 365 | 391 | 532 | 566 | 600 |
| 20 | 365 | 391 | 532 | 559 | 604 |
| 21 | 365 | 396 | 0 | 0 | 0 |
| 22 | 365 | 395 | 533 | 0 | 601 |
| 23 | 365 | 396 | 533 | 0 | 604 |
| 24 | 365 | 391 | 533 | 564 | 595 |
| 25 | 365 | 396 | 534 | 0 | 609 |
| 26 | 366 | 396 | 531 | 565 | 0 |
| 27 | 366 | 396 | 0 | 0 | 604 |
| 28 | 366 | 394 | 0 | 0 | 0 |
| 29 | 366 | 392 | 534 | 0 | 0 |
| Correlation Coefficient ( $E_j$ ) | 0.99999999 | 0.99999997 | 0.99999998 | 0.99999996 | 0.99999992 |
| Skew ( $F_j$ ) | 1.00005291 | 1.00004439 | 1.00000411 | 1.00004903 | 1.00003269 |
| Skew ( $Fp_j$ ) | -53 | -44 | -4 | -49 | -33 |
| Skew error | ±17 | ±30 | ±21 | ±44 | ±61 |

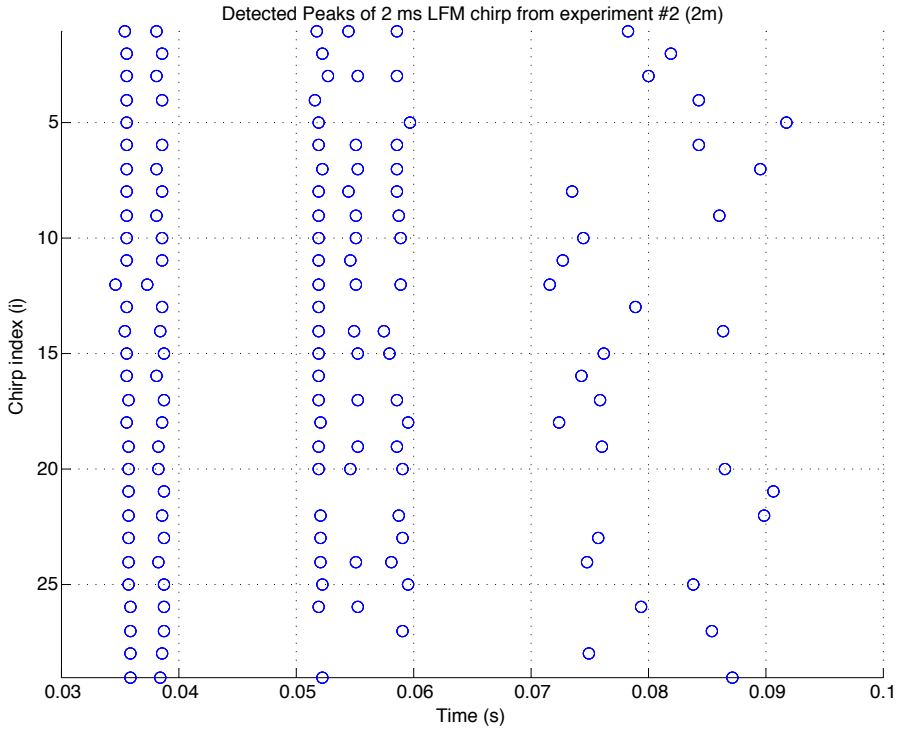


Figure 31. The peak times for an experiment in which clock skew is present: The peak times $u_{ji}$ derived from the ensemble of $n = 30$ measurement signals depicted in Figure 29 are plotted in this figure. Note that each of the $m = 6$ multipath arrivals $a_j, j = 1, 2, \ldots, m$ has a corresponding ensemble $U_j = \{u_{ji}\}_{i=1}^{n}, j = 1, 2, \ldots, m$ associated with it.

Table 5. Detailed results of the 2 ms LFM pulse received during experiment #3, including the correlation coefficient, clock skew (in absolute and ppm values) and its associated error.

| Analysis of 2 ms LFM pulse received during experiment #3 (50 m separation) | | | | | |
|---|---|---|---|---|---|
| Pulse Index | Time index of detected peaks for each multipath | | | | |
| | Detected path #1 | Detected path #2 | Detected path #3 | Detected path #4 | Detected path #5 |
| 1 | 1115 | 1349 | 1405 | 0 | 0 |
| 2 | 1115 | 1357 | 1406 | 1450 | 1523 |
| 3 | 1115 | 1353 | 1402 | 0 | 0 |
| 4 | 1116 | 1358 | 1401 | 0 | 1526 |
| 5 | 1116 | 1355 | 1408 | 1451 | 0 |
| 6 | 1116 | 1351 | 1401 | 0 | 1529 |
| 7 | 1116 | 1350 | 1408 | 1451 | 1524 |
| | Time index of detected peaks for each multipath | | | | |

| Pulse Index | Detected path #1 | Detected path #2 | Detected path #3 | Detected path #4 | Detected path #5 |
|---|---|---|---|---|---|
| 8 | 1116 | 0 | 1408 | 1451 | 1524 |
| 9 | 1116 | 1352 | 1408 | 1451 | 0 |
| 10 | 1116 | 0 | 1413 | 1443 | 1524 |
| 11 | 1116 | 1358 | 1408 | 0 | 0 |
| 12 | 1116 | 1351 | 1410 | 0 | 0 |
| 13 | 1116 | 1351 | 1403 | 1445 | 1524 |
| 14 | 1116 | 1352 | 0 | 1452 | 1519 |
| 15 | 1117 | 1354 | 1404 | 0 | 0 |
| 16 | 1117 | 0 | 0 | 1453 | 0 |
| 17 | 1117 | 1354 | 1412 | 1453 | 0 |
| 18 | 1117 | 1355 | 1406 | 0 | 1524 |
| 19 | 1117 | 1352 | 0 | 1453 | 0 |
| 20 | 1117 | 1352 | 1405 | 0 | 1526 |
| 21 | 1118 | 1355 | 0 | 1451 | 1527 |
| 22 | 1118 | 1352 | 1409 | 1449 | 0 |
| 23 | 1118 | 1352 | 0 | 1453 | 1527 |
| 24 | 1118 | 1352 | 1412 | 1453 | 0 |
| 25 | 1118 | 1352 | 1405 | 1454 | 1525 |
| 26 | 1118 | 0 | 1412 | 1448 | 1529 |
| 27 | 1118 | 1352 | 1409 | 1450 | 1519 |
| 28 | 1118 | 1352 | 1414 | 0 | 1529 |
| 29 | 1118 | 1357 | 0 | 0 | 0 |
| Correlation Coefficient ( $E_j$ ) | 1 | 0.9999987 | 0.9999977 | 0.9999978 | 0.9999980 |
| Skew ( $F_j$ ) | 1.0000450 | 0.9999948 | 1.0000869 | 1.0000336 | 1.0000205 |
| Skew ( $Fp_j$ ) | -45 | 5 | -87 | -34 | -21 |
| Skew error | ±3 | ±23 | ±32 | ±35 | ±36 |

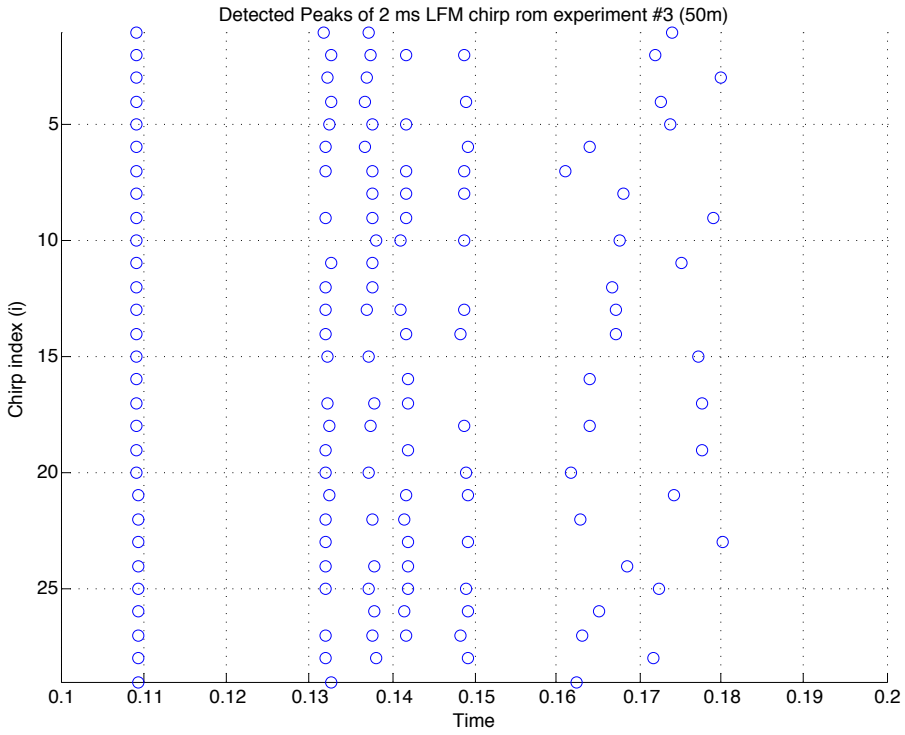


Figure 32. The peak times for an experiment in which clock skew is present: The peak times $u_{ji}$ derived from the ensemble of $n = 30$ measurement signals depicted in Figure 30 are plotted in this figure. Note that each of the $m = 6$ multipath arrivals $a_j, j = 1, 2, \ldots, m$ has a corresponding ensemble $U_j = \{u_{ji}\}_{i=1}^{n}, j = 1, 2, \ldots, m$ associated with it.

The gradual decrease in stability of each successive detected path is also illustrated in Tables 4 and 5. Unlike the first path which is most likely the direct path between the two nodes, the following ones bounced off either or both the surface and the bottom of the lake, inducing variability in the arrivals.

Figure 33 represents the received matched-filtered 10 ms CW signal recorded in experiment #3. This demonstrates the importance of selecting a probe signal which can be easily distinguished by the receiver. Although there is a general trend in the shape of each response, it is difficult to identify a constant peak over all of them.

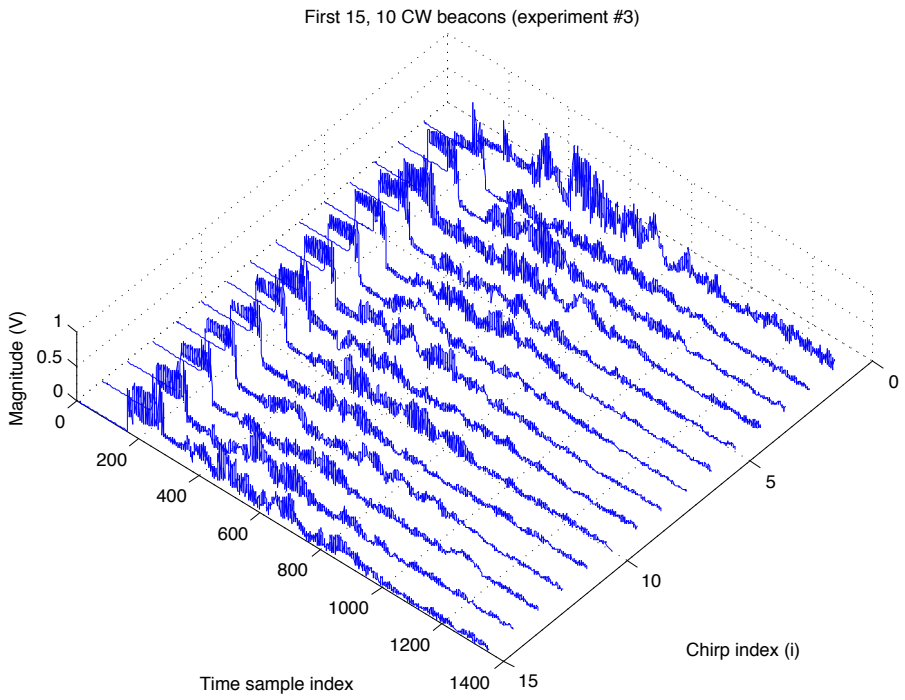


Figure 33. First fifteen 10 ms long CW beacon at 50 m (experiment #2).

Finally, Figure 34 shows the impact of selecting a longer LFM pulse. In this case the main first peak is still clearly identifiable between each chirp, but its general shape is larger and the following chirps are less distinguishable. The combination of the minimal delay difference between the arrivals and the relatively large pulse length probably creates too much superposition to clearly recover subsequent arrivals after the first one.

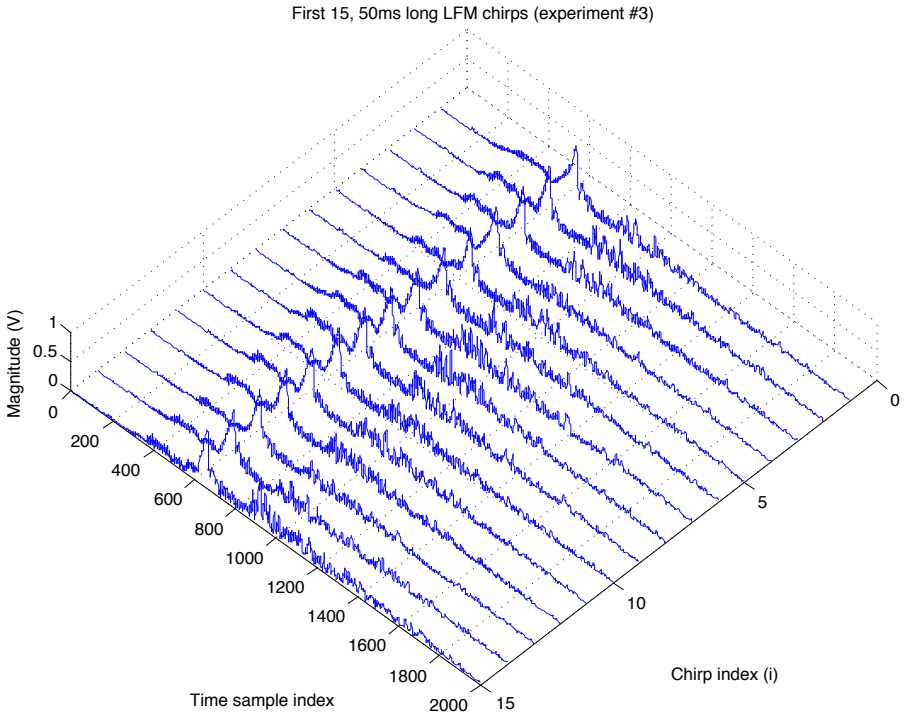


Figure 34. First 15, 50 ms long LFM chirps at 50 m (experiment #3)

Overall, the results from the experiment demonstrate time variability in the tested channel. The first arrival is always present and strong. However, the following arrivals are observed to be gradually less stable as they increasingly interacted with the channel boundaries. The algorithm is able to identify various multipaths based on the detected arrivals and determine the most stable one based on its correlation coefficient. The time indices of these arrivals clearly illustrate the presence of a skew between the two clocks as the time index of the main arrival slowly shifts to the right, as shown in Tables 4 and 5 and the associated Figures 31 and 32. The variance of the results in Table 3 could be due the short period of time over which the chirps are transmitted.

THIS PAGE INTENTIONALLY LEFT BLANK

# VII. CONCLUSION AND RECOMMENDATIONS

In this research we addressed the problem of clock synchronization in an underwater acoustic network. This is a very actively researched area for every type of communication channel. This is particularly challenging in the underwater acoustic environment due to its high latency characteristics, and it requires the development of a specific clock-synchronization protocol. Most of the approaches found in the literature assumed constant propagation delays between two nodes and ignore time variability of the channel. An overview of how and why time variance exists in the underwater acoustic environment was given and a method to evaluate and mitigate its effects as part of a clock-synchronization protocol was proposed.

The proposed method is divided in two stages. The first stage evaluates the frequency drift between the clocks of two adjacent nodes (called the "skew"), and the second stage estimates the offset between the same two nodes.

The first stage was simulated using a computer model and tested in a small, shallow, fresh water lake. Both simulated and experimental results show the effectiveness of the proposed method. However, further testing needs to be done on the basis of the following recommendations to address the variability in the estimated skew calculated from the experimental results.

The second stage could only be simulated since an experiment would require modifying the firmware of the modem, which was not readily possible with the Teledyne Benthos acoustic modems. The results from the simulations are in accordance with the predictions from the theoretical model of the proposed method for offset correction.

Additional experiments are required to fully develop the method and select the optimal parameters. Once completely tested, the addition of this capability to an underwater acoustic network will keep the clocks of the nodes synchronized. This synchronization should improve the utility of the network when deployed or used for long periods of time.

The following recommendations do not necessarily result from the simulation and experiments. Some of them are simply aspects that were omitted due to time or resource constraints.

## A. REPRODUCE EXPERIMENT FROM LITERATURE

Most of the literature pertaining to underwater clock synchronization does not describe physical experiments in an actual underwater environment. The simulations reported in [1] and [7] should be reproduced using the protocol explained in this thesis. This would allow for some comparison among the various protocols and confirm that accounting for time variability improves the synchronization of the clocks.

Another approach to compare the different protocols is to reproduce our experiment using the protocols from [1] and [7].

## B. PSEUDORANDOM BINARY SEQUENCE (PRBS)

Another type of pulse used in channel sounding is the pseudorandom binary sequence (PRBS) [10]. Just as the LFM chirp, the PRBS is characterized by its narrow ambiguity function, making it an excellent choice for measuring the impulse response of a channel. Its structure allows it to be more tolerant to superposition. The generation of a PRBS signal is not complicated and reproducing the experiment from Chapter VI would require minimal effort.

## C. LONGER RPI

As discussed in Chapter VI, the variability of the results shown in Table 3 might originate from a short RPI. The experiment should be reproduced using a constant 2 ms LFM chirp while increasing the RPI duration. This would confirm our hypothesis that the results would improve with a longer RPI.

## D. OFFSET CORRECTION EXPERIMENT

The simulation proves the theory of the offset correction algorithm. However, an experiment in the underwater environment can possibly highlight any neglected factors as was shown when testing our skew-correction algorithms. As stated earlier, technical and

time limitations prevented us from testing our offset correction algorithm in Del Monte Lake. An experiment should be designed and conducted to test the developed algorithm for offset correction described in Chapter IV and simulated in Chapter V.

## E. MORE REALISTIC ENVIRONMENT

Del Monte Lake was selected mostly for its accessibility. As stated in Chapter III, the effects of time variability are location dependent. Since a shallow fresh water lake is not a probable environment where an underwater acoustic network would be deployed, the experiment should be reproduced in an environment more typical of where a time-synchronization protocol would be required and beneficial.

One of the advantages of Del Monte Lake was its low noise level. This will not necessarily be true in an ocean environment. Future work should involve folding measurement noise into the model for skew and offset. Also, noise reduction algorithms should be explored.

## F. DETECTED ARRIVALS SORTING ALGORITHM

The current algorithm is vulnerable to noise and superimposed arrivals. Future work should explore new algorithms to cope with these issues.

THIS PAGE INTENTIONALLY LEFT BLANK

# LIST OF REFERENCES


[1] A.A Syed and J. Heidemann, "Time Synchronization for High Latency Acoustic Networks," in *Proc. IEEE Conference on Computer Communications (Infocom)*, Barcelona, Spain, Apr. 2006.

[2] D.L. Mills, "Modelling and Analysis of Computer Network Clocks," *Technical Report, 92-5-2,* Electrical Engineering Department, University of Delaware, May 1992.

[3] Y.-C. Wu, et al., "Clock synchronization of wireless sensor networks," *IEEE Signal Processing Mag.,* vol 28, no. 1, pp. 124 – 138, Jan. 2011.

[4] J.R. Vig, "Introduction to quartz frequency standards," Army Research Laboratory Electronics and Power Sources Directorate, *Tech. Rep. SLCET-TR-92-1*, Oct. 1992.

[5] *ATM-900 Series Acoustic Telemetry Modems User's Manual*, Rev. B, Teledyne Benthos Inc., North Falmouth, MA, 2012.

[6] B. Sundararaman, et al., "Clock Synchronization for Wireless Sensor Networks: A Survey," *Ad Hoc Networks* (Elsevier), Mar. 2005.

[7] T.-U.I. Khandoker, et al., "A Low Complexity Linear Regression Approach to Time Synchronization in Underwater Networks," *International Conference on Information, Communications and Signal Processing,* Singapore, Dec. 2011.

[8] M. Maroti, et al., "The Flooding Time Synchronization Protocol," in *Proc. 2nd Int. Conf. Embedded Networked Sensor Systems,* ACM Press, Nov. 2004.

[9] M. Stojanovic and J. Preisig, "Underwater Acoustic Communication Channels: Propagation Models and Statistical Characterization", *IEEE Communications Magazine*, Jan. 2009.

[10] P.V. Walree, *Channel sounding for acoustic communications: techniques and shallow-water examples*, report from Norwegian Defence Research Establishment (FFI), Apr. 2011.

[11] X. Lurton, "Environment variability and signal fluctuations", in *An Introduction to Underwater Acoustics, Principles and Applications*, Chichester, UK: Praxis, pp. 128-129, 2002.

[12] J. Preisig, "Surface wave focusing and acoustic communications in the surf zone", *Journal of Acoustical Society of America*, Pt. 1, Oct. 2004.

[13] J. Preisig, "Acoustic Propagation Considerations for Underwater Acoustic Communications Network Development," *WUWNet'06*, Los Angeles, California, Sep. 2006.

[14] J.R. Taylor, "Least-Squares Fitting," in *An introduction to Error Analysis*, 2nd ed. Sausalito, CA: University Science Books, pp. 181-190, 1997.

[15] C.H. Knapp and C. Carter, "The Generalized Correlation Method for Estimation of Time Delay," *IEEE Transaction on Acoustics, Speech, and Signal Processing*, vol ASSP-24, no. 4, Aug. 1976.

[16] J.V. Candy, et al., "Time reversal processing for an acoustic communication experiment in a highly reverberant environment," *JASA*, vol. 115, no. 4, Apr. 2004.

[17] *The BELLHOP Manual and User's Guide,* Preliminary draft, Heat, Light, and Sound Research Inc., La Jolla, CA, 2011.

[18] J.C. Peterson and M.B. Porter. (2011, Jul. 8). *Virtual Timeseries EXperement (VirTEX) – Quick Start* [online]. Available: http://oalib.hlsresearch.com/Rays/VirTEX/README.pdf

[19] B.W. Silverman, "*Density Estimator for Statistics and Data Analysis*," London, UK: Chapman & Hall/CRC, 1998.

[20] Google Earth. (2012, May 5). Aerial view of Del Monte Lake [online]. Available: http://maps.google.com

[21] National Oceanic and Atmospheric Administration, "http://www.noaa.gov".

[22] L.J. Ziomek, "Signal Processing," in *Fundamental is Acoustic Field Theory and Space-Time Signal Processing,* Boca Raton,FL: CRC, pp. 637, 1995.

# INITIAL DISTRIBUTION LIST

1. Defense Technical Information Center
   Ft. Belvoir, Virginia

2. Dudley Knox Library
   Naval Postgraduate School
   Monterey, California

3. Professor Joseph A. Rice
   Naval Postgraduate School
   Monterey, California

4. Dr. Grace A. Clark
   Lawrence Livermore National Laboratories
   Livermore, California

5. Professor Roberto Cristi
   Naval Postgraduate School
   Monterey, California

6. Professor Daphne Kapolka
   Naval Postgraduate School
   Monterey, California

7. Professor R. Clark Robertson
   Naval Postgraduate School
   Monterey, California

8. RADM Gerald Ellis
   Naval Postgraduate School
   Monterey, California

9. RADM Rick Williams
   Naval Postgraduate School
   Monterey, California

10 CAPT Jeff Kline
   Naval Postgraduate School
   Monterey, California

11. Prof Andres Larraza
    Naval Postgraduate School
    Monterey, California

Dale Green
Teledyne Benthos
Falmouth, MA

Mike Coryer
Teldyne Benthos
Falmouth, MA

Ken Scussel
Teledyne Benthos
Falmouth, MA

Bob Headrick
ONR
Arlington, VA

Dave Johnson
ONR
Arlington, VA

Dr. Stephen Potashnik
ONR
Arlington, VA

Dave Jackson
ONI
Washington, DC

Tom Tomaiko
DHS
Alexandria, VA

Chris Fletcher
SSC Pacific
San Diego, California

Bob Creber
SSC Pacific
San Diego, California

Jerry DeJaco
SSC Pacific
San Diego, California

23 Gary Wilson
ARL:UT
Austin, TX

24 Marti Barlett
ARL:UT
Austin, TX

25 Cdr Keith Coffen
MEPM(SM)
Ottawa, Ontario, Canada

26 Gary Heard
DRDC(A)
Halifax, Nova-Scotia, Canada

27 Carmen Lucas
DRDC(A)
Halifax, Nova-Scotia, Canada